OFDM Inspired Waveforms for 5G

Behrouz Farhang-Boroujeny and Hussein Moradi

***Abstract*—As the standardization activities are being formed to lay the foundation of 5G wireless networks, there is a common consensus on the need to replace the celebrated orthogonal frequency division multiplexing (OFDM) by a more effective air interface that better serves the challenging needs of 5G. To this end, in the recent past, a number of new waveforms have been introduced in the literature. Interestingly, and at the same time not surprising, these methods share a common fundamental principle with OFDM: each data packet is made up of a number of complex-valued sinusoidals (pure tones) that are modulated by the information symbols. In this tutorial article, we build a common framework based on the said OFDM principle and derive these new waveforms from this point of view. This derivation provides a new perspective that facilitates straightforward understanding of channel equalization and the application of these new waveforms to multiple-input multiple-output channels. It also facilitates derivation of new structures for more efficient synthesis/analysis of these waveforms than those that have been reported in the literature.**

***Index Terms*—Wireless communication, physical layer, multicarrier communication, OFDM, filter bank multicarrier.**

I. Introduction

In THE past, orthogonal frequency division multiplexing (OFDM) has enjoyed its dominance as the most popular signaling method in broadband wired [1], [2], and wireless [3], [4], channels. OFDM has been adopted in the broad class of digital subscriber line (DSL) standards, as well as in the majority of wireless standards, e.g., variations of IEEE 802.11 and IEEE 802.16, the third generation partnership program long-term evolution (3GPP-LTE), and LTE-Advanced. OFDM is known to be a perfect choice for point-to-point and downlink communications. It offers a minimum complexity and achieves good bandwidth efficiency. The low complexity of OFDM is a consequence of the fact that each OFDM symbol is synthesized as a summation of a number of *pure tones* (complex-valued sinusoidal signals) that are modulated by a set of quadrature amplitude modulated (QAM) data symbols. Moreover, channel distortion is taken care of trivially by adding a cyclic prefix (CP) to each OFDM symbol.

Manuscript received December 17, 2015; revised March 27, 2016; accepted May 1, 2016. Date of publication May 12, 2016; date of current version November 18, 2016. This work was supported in part by the Battelle Energy Alliance LLC through the U.S. Department of Energy under Contract DE-AC07-05ID14517, and in part by Idaho National Laboratory under Grant INL/JOU-14-33556. The U.S. Government retains and the publisher, by accepting the article for publication, acknowledges that the U.S. Government retains a nonexclusive, paid-up, irrevocable, world-wide license to publish or reproduce the published form of this manuscript, or allow others to do so, for U.S. Government purposes.

B. Farhang-Boroujeny is with the Electrical and Computer Engineering Department, University of Utah, Salt Lake City, UT 84112 USA (e-mail: farhang@ece.utah.edu).

H. Moradi is with Idaho National Laboratory, Idaho Falls, ID 83415 USA.

Digital Object Identifier 10.1109/COMST.2016.2565566

It has been noted that OFDM has to face many challenges when considered for adoption in more complex networks. For instance, the use of OFDM in the uplink of multiuser networks, known as OFDMA (orthogonal frequency division multiple access), requires full synchronization of the users' signals at the base station input. Such synchronization has been found very difficult to establish, especially in mobile environments where Doppler shifts of different users are hard to predict/track. Morelli *et al.* [5] have noted that "*carrier and timing synchronization represents the most challenging task in OFDMA systems.*" To combat the problem, in LTE and LTE-Advanced resource intensive close-loop procedures have been included to achieve the tight synchronization requirements. On the other hand, some researchers have relaxed on the need for a close to perfect carrier synchronization among users, and have proposed multiuser interference cancellation methods [6]–[9]. These methods are generally very complex to implement. Their implementation increases the receiver complexity by orders of magnitude [10]. These solutions are either too slow and/or too resource intensive to be of interest in many applications of 5G where low cost devices need to communicate.

Another limitation of OFDM appears when attempt is made to transmit over a set of non-contiguous frequency bands. The poor response of the subcarrier filters in IFFT/FFT (inverse fast Fourier transform/fast Fourier transform) filter banks of OFDM introduces significant out of band *egress noise* to other users and also picks up significant *ingress noise* from them. The same problem appears if one attempts to adopt OFDM for filling in the spectrum holes in cognitive radios. Methods of reducing OFDM spectral leakage (also known as out-of-band (OOB) emissions) have been proven to be very limited in performance. For instance, the side lobe suppression techniques, like those proposed in [11]–[13], can achieve an out of band emission suppression of only 5 to 10 dB, while incur some loss in bandwidth efficiency and add significant complexity to the transmitter.

Filter bank multicarrier (FBMC) is an alternative transmission method that resolves the above problems by using high quality filters that avoid both ingress and egress noise. Also, because of the very low out of band emission of the subcarrier filters, application of FBMC in the uplink of multiuser networks is trivial [14], [15]. Accordingly, FBMC can be deployed without synchronization of mobile user nodes. In the application of cognitive radios, the filter bank that is used for multicarrier data transmission can also be used for spectrum sensing [16]–[21]. On the other hand, compared to OFDM, FBMC falls short in handling multiple-input multiple-output (MIMO) channels, although a few solutions to adopt FBMC in MIMO channels have been reported in [22]–[24],

and research in this domain still continues. Moreover, the ramp-up and ramp-down of an FBMC signal at the beginning and the end of each packet, respectively, can lead to a significant loss in bandwidth efficiency when the data packets are short. Unfortunately, this can be problematic, at least, in part of 5G applications where machine-to-machine (M2M) communications and Internet of Things (IoT) involve exchange of very short messages and possibly with a very short latency.

Following the above arguments, it is obvious that none of the existing waveforms are sufficient to serve all aspects of the 5G. Noting this, in recent past, a number of attempts have been made to propose waveforms that resolve the problems of both OFDM and FBMC. Generalized frequency division multiplexing (GFDM) that was first introduced in 2009 by Fettweis *et al.* [25] is an improvement to OFDM in which filtering is imposed on each subcarrier band to minimize the overlapping among subcarriers, thus facilitate multiuser application without worrying about accurate synchronization of the users. Moreover, the waveform design in GFDM is such that one may choose to use one CP for many symbols or only one CP for the whole packet, assuming that channel variation over each packet remains negligible. This can improve the bandwidth efficiency of the packetized data transmissions significantly. The down side of these changes is that adjacent subcarriers suffer from some level of interference whose compensation adds some complexity to the receiver and may incur some loss in performance. The term *non-orthogonal waveform* is often used to refer to this property of GFDM [26]. Since its invention in 2009, a broad set of papers have explored different aspects of GFDM, e.g., [27]–[32]. A summary of these works have been collected and reported in [26].

More recently, it has been noted that the concept based on which GFDM waveform is built can be extended to FBMC [33]–[36]. The waveform that results from this extension may be called circular FBMC (C-FBMC) because of the reasons that become obvious later. Interestingly this extension preserves the orthogonality of the subcarrier symbols, hence, no complicated intercarrier interference (ICI) cancellation processing is necessary and, consequently, any loss in performance is avoided. Another interesting outcome of C-FBMC waveform is that its extension to MIMO channels is found straightforward, in the same way as GFDM. Although, there are multiple publications in the literature that talk about extension of GFDM/C-FBMC to MIMO channels, see [26], the trivial solution that is presented in this article is from one of our recent publications [37].

Another relevant work that should be acknowledged here is the so called cyclic block filtered multitone (CB-FMT) [38]–[40]. This method also builds its waveform following the same principle as GFDM and C-FBMC. However, unlike GFDM and C-FBMC which allow some overlap of adjacent subcarrier bands, hence achieve full bandwidth efficiency, CB-FMT is constructed such that adjacent subcarrier bands do not overlap. This, obviously, results in some bandwidth efficiency loss. To keep the content of this article concise, no further details of CB-FMT is pursued here. Lin and Siohan [36], have already provided a detailed comparison of CB-FMT and C-FBMC methods.

Beside the above new waveforms, over the years, many other attempts have been made to resolve the previously discussed deficiencies of OFDM as well as to add more features to it. In particular, windowed OFDM and filtered OFDM have been proposed to resolve the problem of spectral leakage and, thus, allow some relaxation on synchronization needs in OFDM-based networks. Both methods can be categorized as filtering operations that reduce the OOB emissions. While the windowed OFDM has been adopted in DSL technologies and in IEEE 802.11 standards, the filtered OFDM has been selected for IEEE 802.16 standards as well as LTE and LTE-advanced. We will elaborate on these techniques later and show that such filtering methods are also necessary for effective operations of GFDM and C-FBMC. Other developments have been made to improve OFDM for other reasons. For instance OFDM with DFT pre-coding (known as single carrier frequency division multiple access (SC-FDMA)) has been proposed and adopted in LTE and LTE-advanced to overcome the high peak-to-average-power-ratio (PAPR) of OFDM in uplink of OFDMA networks [41], [42]. An improved form of SC-FDMA, named zero-tail DFT-spread OFDM (ZT-DFT-s-OFDM), has been proposed in [43]. ZT-DFT-s-OFDM is designed to suppress the signal level at the two sides of each OFDM symbol, to allow more tolerance to timing mis-match among multiple users in an OFDMA network. Another interesting development is the unique word OFDM (UW-OFDM) [44]–[46]. The UW-OFDM removes the CP of OFDM, but instead encodes a reduced set of QAM symbols to an OFDM (super-)symbol. This encoding introduces some redundancy that the receiver can benefit from for a more reliable detection of the transmitted QAM symbols. It also suppresses a few of the samples at the end of each OFDM symbol to zeros. These zeros are then replaced a predefined sample set which is called *unique word*. In some other works, it has been noted that one may replace the CP in the conventional OFDM by a set of zero samples. This is referred to as zero-padded OFDM (ZP-OFDM) [47], [48]. Moreover, it has been noted that the zero samples in ZP-OFDM may be replaced by a known sequence and the result has been referred to as known symbol padded OFDM (KSP-OFDM) [49]–[52]. Furthermore, it has been noted that the unique word in UW-OFDM and the known symbol sequence in KSP-OFDM may be used for synchronization purposes at the receiver. This article does not intend to discuss these variations of OFDM any further, although these may also be potential candidates for 5G. Nevertheless, comments will be made in later parts on possible extension of some of the underlying concepts to GFDM and C-FBMC.

Another candidate for 5G that has recently been proposed by a number of researchers from the Alcatel-Lucent Bell Laboratories is universal filtered OFDM (UF-OFDM) [53]–[57]. UF-OFDM has also been referred to by the name universal filtered multicarrier (UFMC). UF-OFDM is in effect a combination of ZP-OFDM and filtered OFDM. The CP in the conventional OFDM is forced to a set of zero samples and the result, for each allocation of

a single user, is passed through a bandpass filter to suppress the OOB emissions. This, clearly, reduces the multiuser interference. The CP interval, which is replaced by zeros, is used to absorb the transient interval that results from the use of the bandpass filters. In the absence of a multipath channel, UF-OFDM holds the orthogonality of the subcarriers of each user perfectly and approximately among different users. However, as the time spreading of underlying channels increases, the orthogonality assumption among subcarriers of each user as well as among different users becomes less accurate. In light of this property, UF-OFDM may also be categorized as a non-orthogonal multicarrier technique. However, the level of non-orthogonality in UF-OFDM is significantly lower than GFDM and it varies with the channel. As a result, one may find that the name *quasi-orthogonal* better suits this particular feature of UF-OFDM.

We note that the goal of this article is not to critically compare the various waveforms that have recently been proposed and are under study for 5G. Such comparison requires a broad set of theoretical studies and numerical simulations that fall beyond the scope of this tutorial article. Our presentation is to provide a review of the new candidate waveforms and, in particular, present GFDM and C-FBMC from a point of view that reveals their close similarity to OFDM. We note that both waveforms are synthesized by adding a finite number of pure tones, exactly in the same way that OFDM waveform is constructed. The difference is that while in OFDM each symbol modulates a single tone, in GFDM and C-FBMC each symbol modulates multiple tones. And it is the combination of the respective tones that (when done properly) confines each subcarrier to the intended bandwidth. The point of view that is presented in this article also reveals a close similarity of GFDM and C-FBMC and the fact that any advancement in one may be extended to the other. In addition, we review some interesting features of UF-OFDM which facilitate its comparison with GFDM and C-FBMC. Moreover, our presentation allows us to explain the extension of GFDM, C-FBMC and UF-OFDM to MIMO channels straightforwardly. Furthermore, we take note of the fact that the concept based on which UF-OFDM is constructed can be applied to GFDM/C-FBMC to introduce an improved class of waveforms for 5-G.

This article is organized as follows. In Section II, we highlight the fundamental principle based on which OFDM waveform is constructed. Next, in Section III, we introduce a less understood, but the relevant concept of *frequency spreading design of digital filters*. We combine the results of Sections II and III to introduce a new construction for GFDM waveform in Section IV. The transmitter and receiver implementations of GFDM are also discussed in this section. Moreover, we show the same principle based on which MIMO communication is formed in OFDM is applicable to GFDM. In Section V, we show the approach that was used in Section IV is readily applicable to the construction of the respective FBMC waveform, *viz.,* C-FBMC. UF-OFDM is reviewed in Section VI. We find that due to the removal of CP, UF-OFDM deviates from the said OFDM principle. That is, from the receiver detector point of view, data symbols may no longer be carried over pure tones. Nevertheless, data symbols separation and MIMO processing, as in OFDM, is possible by making use of an FFT with twice the size of the one in OFDM. Multiuser networks and the relevant discussions associated with the waveforms that are reviewed in these papers are presented in Section VII. The concluding remarks and suggestions for further works are presented in Section VIII.

Notations: Our presentation in this article is through a mix of continuous time and discrete time signals. We use (t) to denote the continuous time variable and $[n]$ to denote discrete time index. Subcarrier index is denoted by subscript k. Discrete time index, n, when has to be added to a continuous time function is put as a subscript, e.g., $x_n(t)$. Bold lower case is used for column vectors and bold upper case for matrices. All vectors are in column form. E$[\cdot]$ denotes statistical expectation. The vector and matrix transpose and Hermitian are indicated by the superscripts 'T' and 'H', respectively. We use $\mathcal{F}_N$ to denote discrete Fourier transform (DFT) matrix of size N. We also assume that $\mathcal{F}_N$ is normalized, such that $\mathcal{F}_N\mathcal{F}_N^{\mathrm{H}} = \mathbf{I}_N$, where $\mathbf{I}_N$ denotes the identity matrix of size N. Hence, $\mathcal{F}_N^{-1}$ and $\mathcal{F}_N^{\mathrm{H}}$ are equal and both denote the inverse DFT (IDFT) matrix of size N, and these may be used interchangeably. The terms FFT and IFFT refer to the fast implementations of DFT and IDFT, respectively.

II. The OFDM Principle

Each OFDM symbol carries N QAM symbols $s_k[n]$, $k = 0, 1, \ldots, N-1$, and is constructed as

$$x_n(t) = \sum_{k=0}^{N-1} s_k[n] e^{j\frac{2k\pi}{T}t}. \tag{1}$$

Related to (1), there are a few points that should be noted:

1) $x_n(t)$ is a summation of N tones, weighted by the data symbols $s_k[n]$.
2) These tones are spaced at $F = 1/T$ and are located at the frequencies $f = 0,\ 1/T,\ 2/T,\ \ldots,\ (N-1)/T$.
3) $x_n(t)$ is periodic with a period of T.
4) The Fourier series coefficients of $x_n(t)$ are the data symbols $s_k[n]$, $k = 0, 1, \ldots, N-1$, and the construction of $x_n(t)$ may be viewed as an inverse Fourier series.
5) If $x_n(t)$ is passed through a channel with the transfer function $H(f)$, the channel output, excluding its transient response, is obtained as

$$y_n(t) = \sum_{k=0}^{N-1} H\left(\frac{k}{T}\right) s_k[n] e^{j\frac{2k\pi}{T}t}. \tag{2}$$

6) Obviously, $y_n(t)$ is also periodic with a period of T.
7) The Fourier series coefficients of $y_n(t)$ are $H\left(\frac{k}{T}\right)s_k[n]$, $k = 0, 1, \ldots, N-1$. Hence, the transmitted data symbols $s_k[n]$ can be extracted from samples of $y_n(t)$, by applying a Fourier series analysis and equalizing the results by the inverse of channel gains at the respective frequencies.

In practice, where a digital circuitry or a software radio is used for implementation, (1) is implemented through an inverse discrete Fourier transform, or equivalently and conveniently, through an IFFT. IFFT output delivers only one cycle of the sampled version of $x_n(t)$; say $x_n[m]$, for

$m = 0, 1, \ldots, N-1$. Similarly, the data extraction at the receiver is performed by applying an FFT to the samples of a single period of $y_n(t)$, say, $y_n[m]$, for $m = 0, 1, \ldots, N-1$, and equalizing the results by multiplying to the inverse of the channel gains, as noted in item 7), above.

Clearly, it will be resource inefficient to transmit $x_n(t)$ for any period of time beyond the minimum duration that one needs for correct extraction of the data symbols $s_k[n]$ at the receiver. This minimum duration is T (one period of $x_n(t)$) plus the duration of the channel impulse response, T_{ch}. The latter is needed to absorb the channel transient response. To serve this purpose, in digital implementation of the transmitter, a number of samples, equivalent to $T_{\text{cp}} \geq T_{\text{ch}}$, from the end of the IFFT output are prefixed to its beginning. The prefixed samples, because of obvious reasons, are called *cyclic prefix* (CP). At the receiver, the FFT is applied after removing the CP samples.

From the above discussion, it follows that each OFDM symbol has a duration of $T + T_{\text{cp}}$, and a data packet consisting of M OFDM symbols may be expressed, in continuous time, as

$$\begin{aligned} x(t) &= \sum_{n=0}^{M-1} x_n\big(t - T_{\text{cp}} - n\big(T + T_{\text{cp}}\big)\big) \\ &= \sum_{n=0}^{M-1} s_k[n] e^{j\frac{2\pi}{T}\left(t - T_{\text{cp}} - n\left(T + T_{\text{cp}}\right)\right)}. \end{aligned} \tag{3}$$

To facilitate our discussions in the subsequent parts of this article, we have presented in Fig. 1 the structure of an OFDM packet. As follows from the above discussion, each OFDM symbol (consisting of N QAM symbols) needs to be cyclic prefixed.

III. Frequency Spreading Design of Digital Filters

Matrin [58] suggested a method of designing a class of finite impulse response (FIR) square-root Nyquist (N) filters whose impulse response is expressed as

$$p[n] = \begin{cases} c_0 + 2\sum_{l=1}^{M-1} c_l \cos\left(\frac{2\pi ln}{L}\right), & 0 \leq n \leq L-1 \\ 0, & \text{otherwise} \end{cases} \tag{4}$$

where $L = MN$ is the filter length, N is the spacing between zero-crossings of Nyquist pulse-shape $q[n] = p[n] \star p[-n]$, and the parameter M is referred to as *overlapping factor*. Mirabbasi and Martin [59], later, presented an improved design over that of [58].

We also note that (4) may be rearranged as

$$p[n] = \sum_{l=0}^{L-1} \tilde{c}_l e^{j\frac{2\pi ln}{L}} \tag{5}$$

where

$$\tilde{c}_l = \begin{cases} c_l, & 0 \leq l \leq M-1 \\ 0, & M \leq l \leq L-M \\ c_{L-l}, & L-M+1 \leq l \leq L-1. \end{cases} \tag{6}$$

This observation implies that in the frequency domain, over a grid of L frequency bins, $p[n]$ is characterized by the $2M-1$ non-zero coefficients $\tilde{c}_l$ or, equivalently, $2M-1$ complex frequency bins/tones. According to [58] and [59], the choices of $M \geq 4$ usually lead to very good designs with stopband attenuations of over 70 dB.

Next, consider the case where $p[n]$ is used as the prototype filter to realize a filter bank consisting of N subbands centered at the normalized frequencies $f_0 = 0, f_1 = \frac{M}{L} = \frac{1}{N}, f_2 = \frac{2M}{L} = \frac{2}{N}, \ldots, f_{N-1} = \frac{(N-1)M}{L} = \frac{N-1}{N}$. The k-th modulated filter of this filter bank is characterized by the impulse response

$$\begin{aligned} p_k[n] &= p[n] e^{j2\pi f_k n} \\ &= \sum_{l=0}^{L-1} \tilde{c}_l e^{j\frac{2\pi(Mk+l)n}{L}} \\ &= \sum_{l=0}^{L-1} \tilde{c}_{(l-Mk)_L} e^{j\frac{2\pi ln}{L}}. \end{aligned} \tag{7}$$

where $(\cdot)_L$ means modulo L. The result in (7) shows that each of the modulated filters in the filter bank is characterized by $2M-1$ non-zero coefficients/tones. These coefficients are obtained through circular shift of the coefficients $[\tilde{c}_0, \tilde{c}_1, \ldots, \tilde{c}_{L-1}]$ of the prototype filter $p[n]$ in (5). We will make use of this property of the prototype filter $p[n]$ in the following sections to propose effective implementations for the transmitter and receiver of GFDM and C-FBMC. Lastly, we note from (7) that the DFT coefficients of the time sequence $p_k[n]$ (equivalently, the corresponding subband frequency response) are all zero, except those that lie within its passband.

IV. GFDM

A. Derivation

As opposed to OFDM, packet construction in GFDM is such that only one CP may be sufficient to take care of the channel transient response. Fig. 2 presents the structure of a GFDM packet, as given in [25]–[32]. For the reasons that are explained below, we refer to the collection in Fig. 2 as a GFDM *block,* and leave the term *'packet'* for a collection of blocks. The data symbols are spread across time and frequency, as in OFDM. However, the data stream in each subcarrier is controlled through a filter which confines its frequency response to a limited bandwidth. Similar to OFDM, the data symbols (the columns of a GFDM block) are transmitted at an interval T and subcarrier spacing is set equal to $F = 1/T$.

As will be shown later, the detection of data symbols that are carried within each GFDM block is only possible after receiving the complete set of samples of the block. Hence, when dealing with long packets of data, it may be unreasonable to put the whole packet in one block, as this will introduce a long latency in the detection of the transmitted information at the receiver. Moreover, long blocks can be affected by time-variation of the channel and lead to a significant degradation of the receiver performance. To avoid these problems, a large packet of data should be divided into a number of segments, each of which will be synthesized in one GFDM block. Hence, a complete packet in GFDM may be a concatenation of multiple blocks, as multiple symbols in OFDM. Short packets, like those that may be encountered in M2M communications, may consist of only one block.

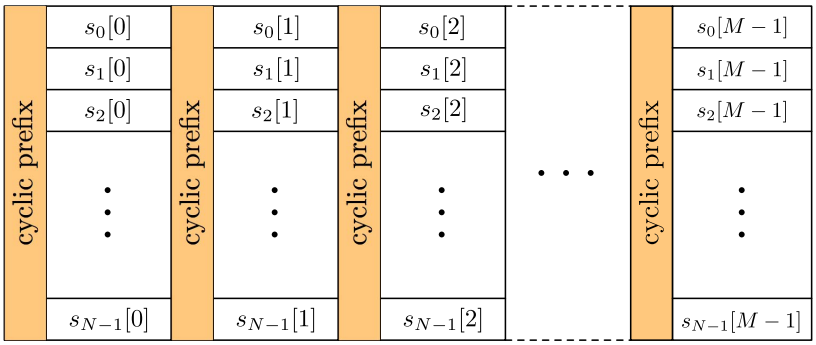

Fig. 1. An OFDM packet.

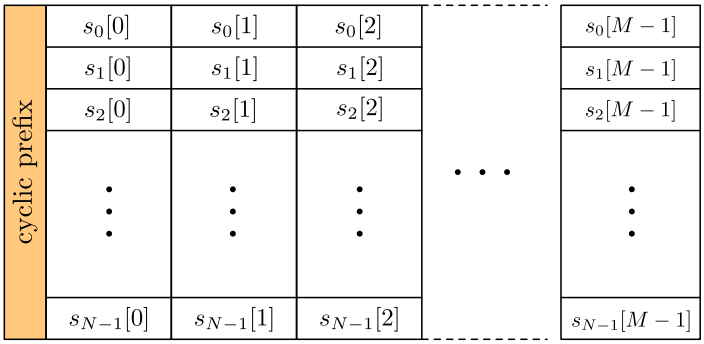

Fig. 2. A GFDM block/packet.

Before we begin our derivation of GFDM, the reader should be reminded that the derivation that follows builds on the frequency spreading design of digital filters that was presented above. This derivation is different from what has appeared in [25]–[32] where GFDM was derived based on circular convolutions. The use of circular convolutions instead of linear convolutions was to construct a periodic signal and, thus, to allow the addition of CP as dictated by the OFDM principle. Our derivation also leads to the same periodic signal, however, at the same time reveals some interesting properties of the GFDM waveform which otherwise were hard to see. Our derivation was first presented in [37].

From the discussion presented above for OFDM, one may deduce that to allow the use of a single CP per GFDM block, the modulated signal that carries all the data symbols in a GFDM block should be a single cycle of a periodic signal with the length of MT. This is indeed the case in GFDM and such a periodic signal is constructed, following the OFDM signal synthesis, according to the formulas that follow. The contribution from the n-th data column in the GFDM block/packet of Fig. 2 is synthesized as

$$x_n(t) = \sum_{k=0}^{N-1} \sum_{l=0}^{L-1} s_k[n] \tilde{c}_{(l-Mk)_L} e^{j\frac{2\pi l}{MT}(t-nT)}. \tag{8}$$

Note that this synthesizes the data symbols $s_0[n]$ through $s_{N-1}[n]$ over the N subcarrier bands by following the frequency spreading method of the previous section. We also note that $x_n(t)$, effectively, is the sum of $L = MN$ tones at the frequencies 0, $1/MT$, $2/MT$, $\cdots$. Since all these tones may be considered as periodic with a period of MT, $x_n(t)$ is also periodic with the same period.

The complete waveform carrying all the data symbols in the GFDM block of Fig. 2 is obtained by summing up the result of (8) over $0 \leq n \leq M-1$. That is

$$x(t) = \sum_{n=0}^{M-1} x_n(t). \tag{9}$$

Obviously, since the components $x_n(t)$ are periodic with a period MT, $x(t)$ is also periodic and has the same period. The GFDM block is thus obtained by taking a segment of $x(t)$, of (9), over the interval $-T_{\text{cp}} \leq t \leq MT$.

Following the above concept, synthesizing a block of GFDM in discrete time can be performed according to the schematic diagram shown in Fig. 3. Here, each data symbol $s_k[n]$ is fed into an IFFT block through a number of tones which construct the corresponding subcarrier filter according to the method of frequency spreading (the frequency spreading coefficients $\tilde{c}_l$). The frequency spreading coefficients, in Fig. 3, are signified by the filter responses that indicate the frequency responses of different subcarrier bands. The "circular shift and accumulate" block adds up the results of IFFT for each set of data symbols, after applying a circular shift. The circular shift is to take care of the time delay between the successive data columns, as indicated in the block/packet format of Fig. 2. The delay associated with the symbol set at the time index n in continuous time is nT. In discrete time, this corresponds to nN sample delay/circular shift. Note that this implies there are N samples of $x(t)$ is each symbol period T. Note that

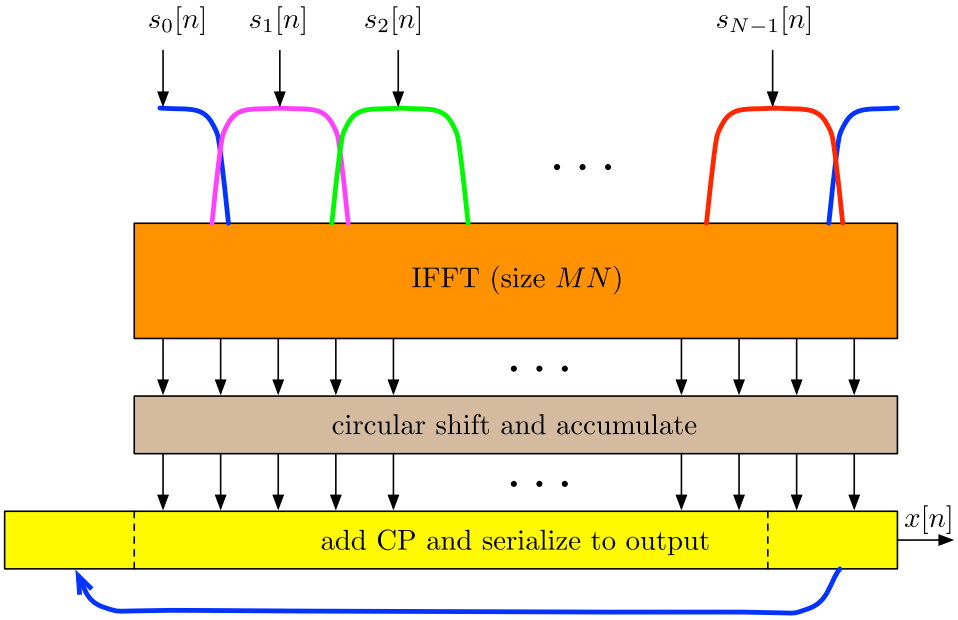

Fig. 3. An implementation of GFDM transmitter.

here 'delay' and 'circular shift' are equivalent because of the periodic form of the synthesized signal $x(t)$.

B. Transmitter Implementation

Direct implementation of GFDM transmitter according to the schematic diagram of Fig. 3 requires a total of M IFFT operations of size MN, plus additional operations prior and after IFFT. This complexity can be reduced significantly by some rearrangement of the operations as explained next.

The equation that relates the input data symbols $s_k[n]$ and the IFFT output, denoted by the length MN column vector $\mathbf{x}[n]$, may be expressed as

$$\mathbf{x}[n] = \mathcal{F}_{MN}^{-1}\mathbf{C}\mathbf{s}_{\mathrm{e}}[n] \tag{10}$$

where $\mathbf{s}_{\mathrm{e}}[n] = [s_0[n]\ \mathbf{0}\ s_1[n]\ \mathbf{0}\ \cdots\ s_{N-1}[n]\ \mathbf{0}]^{\mathrm{T}}$, $\mathbf{0}$ is a row of $M-1$ zeros, and

$$\mathbf{C} = \begin{bmatrix} c_0 & c_1 & \cdots & c_{M-1} \\ c_1 & c_0 & \cdots & c_{M-2} \\ \vdots & \vdots & \ddots & \vdots \\ c_{M-1} & c_{M-2} & \cdots & 0 \\ 0 & c_{M-1} & \cdots & 0 \\ \vdots & \vdots & \ddots & \vdots \\ c_{M-1} & 0 & \cdots & c_{M-2} \\ \vdots & \vdots & \ddots & \vdots \\ c_1 & c_2 & \cdots & c_0 \end{bmatrix}.$$

Note that $\mathbf{C}$ is a circular matrix of size $MN \times MN$.

Direct implementation of (10) is performed in two steps:

1) The circular convolution of the first column of $\mathbf{C}$ and the vector $\mathbf{s}_{\mathrm{e}}[n]$ is performed to obtain $\mathbf{C}\mathbf{s}_{\mathrm{e}}[n]$.
2) An IFFT of size MN is applied to the result of step 1) to obtain $\mathbf{x}[n]$.

The complexity of this procedure which should be repeated M times for each block is dominantly determined by Step 2); an IFFT of size MN.

Alternatively, $\mathbf{x}[n]$ may be calculated by arranging (10) as

$$\mathbf{x}[n] = \mathcal{F}_{MN}^{-1}\underbrace{\mathcal{F}_{MN}\left[\left(\mathcal{F}_{MN}^{-1}\mathbf{c}_1\right)\odot\left(\mathcal{F}_{MN}^{-1}\mathbf{s}_{\mathrm{e}}[n]\right)\right]}_{\mathbf{C}\mathbf{s}_{\mathrm{e}}[n]} \tag{11}$$

where $\mathbf{c}_1$ is the first column of $\mathbf{C}$, $\odot$ denotes point-wise multiplication, and the circular convolution of the vectors $\mathbf{c}_1$ and $\mathbf{s}_{\mathrm{e}}[n]$ is performed through point-wise multiplication of their respective IDFTs and then applying a DFT to the result. Here, we have chosen to use IDFT domain instead of the common approach of using DFT domain because this, as explained next, gets us to a low complexity implementation of the transmitter.

Obviously, (11) reduces to

$$\mathbf{x}[n] = \mathbf{p}\odot\left(\mathcal{F}_{MN}^{-1}\mathbf{s}_{\mathrm{e}}[n]\right) \tag{12}$$

where $\mathbf{p} = \mathcal{F}_{MN}^{-1}\mathbf{c}_1$ is the vector of prototype filter coefficients of GFDM in the time domain. We note that the computational complexity of (12) is still dominantly determined by the complexity of the operation $\mathcal{F}_{MN}^{-1}\mathbf{s}_{\mathrm{e}}[n]$, i.e., computation of IFFT of $\mathbf{s}_{\mathrm{e}}[n]$. However, since $\mathbf{s}_{\mathrm{e}}[n]$ is the M-fold expanded version of the length N column vector $\mathbf{s}[n] = [s_0[n]\ s_1[n]\ \cdots\ s_{N-1}[n]]^{\mathrm{T}}$, $\mathcal{F}_{MN}^{-1}\mathbf{s}_{\mathrm{e}}[n]$ can be obtained by M repetitions of $\mathcal{F}_{N}^{-1}\mathbf{s}[n]$, in a column. Hence, following (12), $\mathbf{x}[n]$ can be calculated through an IFFT of size N.

Next, we note that the final content of the circular shift and accumulate block in Fig. 3, upon including all the data symbols of the GFDM block, will be the vector

$$\mathbf{x}_{\mathrm{gfdm}} = \sum_{n=0}^{M-1}\mathrm{circshift}(\mathbf{x}[n], nN) \tag{13}$$

where circshift$(\cdot)$ means downward circular shift. After adding the CP to $\mathbf{x}_{\mathrm{gfdm}}$, we have a complete GFDM block to transmit.

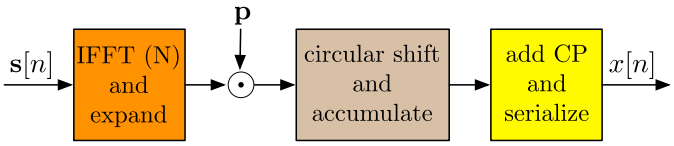

Fig. 4. A simplified implementation of GFDM transmitter.

The results presented in (12) and (13) have the following interpretation. According to (12), each set of data symbols modulate a set of carrier tones that are then added together and the result is shaped by a well designed function defined by the prototype filter **p**. The results for different choices of time index n are subsequently circularly shifted and added together to obtain the vector $\mathbf{x}_{\text{gfdm}}$.

Now considering the results of (12) and (13) and the discussions following these equations, the simplified transmitter block diagram of Fig. 4 is obtained. Following this block diagram, the computation of each GFDM block involves M FFT operations, each of size N, M dot multiplication of **p** by the expanded output of IFFT, and M vector additions. For convenience, as a measure of complexity, each complex multiplication followed by a complex addition is referred to as one operation. Accordingly, the number of operations for IFFTs will be $(MN/2)\log_2 N$. We note that the elements of **p** are real-valued and it has a length of MN. We count each real by complex multiplication as half a complex multiplication. Hence, point-wise multiplications by **p** and additions to the circular shift and add block are counted as $M^2N/2$ operations. Adding our results, we find that the number of operation to calculate each GFDM block will be

$$C_1 = \frac{MN}{2}\log_2 N + \frac{M^2N}{2} \text{ operations.} \tag{14}$$

Taking the formula (7) of [30] (a previous paper on efficient implementation of the transmitter in GFDM) and assuming that the number of active subcarriers is equal to N (i.e., in formula (7) of [30] we have replaced K by N) to match our notation here, the reported result in [30] will be[1]

$$C_2 = \frac{3MN}{2}\log_2 MN + 2MN \text{ operations.} \tag{15}$$

A quick comparison of (14) and (15) reveals that for typical situations where M is not a large number (typically 3 or 5) the implementation proposed here is about three times less complex than that of [30].

At this point, it is important that a comment be made on the impact of an abrupt start of a GFDM packet at the beginning of the preamble and an abrupt stop to the packet at the end of the payload. This is equivalent to applying a rectangular window to the underlying periodic waveform that the GFDM packet originates from. Application of a rectangular window in time translates to a convolution of the spectrum of the periodic waveform with a 'sinc' pulse in the frequency domain. This, in turn, spreads the subcarriers' spectra over the whole of the transmission bandwidth and effectively nullifies the filtering operation that was applied earlier to confine the spectrum of each subcarrier to a limited bandwidth. It also results in a significant OOB emissions. The solution to this problem is trivial. The rectangular window is replaced by a window function with smooth corners at the two sides, e.g., raised-cosine shapes at the beginning and at the end of the packet are applied as in windowed OFDM [19], [20]. Alternatively, a bandpass filter may be applied to each synthesized GFDM signal, as done for OFDM signals in LTE and LTE-Advanced. Moreover, the approach that is taken in UF-OFDM to control the OOB emissions may be applied to GFDM to enhance its performance.

[1] In [30], the number of operations to perform an FFT of size N is assumed to be $N\log_2 N$. Here, we have replaced it with the more accurate figure $(N/2)\log_2 N$ [60].

C. Receiver Implementation

The key idea for development of any receiver implementation for GFDM is to recall that after removing the CP, the received signal vector **y** (of size $MN \times 1$) may be thought as one period of a periodic signal whose spectral contents are those of the transmit signal vector $\mathbf{x}_{\text{gfdm}}$, scaled by the channel gains at the respective frequencies (i.e., the transmitted tones). Channel equalization at the receiver, thus, becomes a trivial task. An FFT is applied to the received vector **y** and each element of the result will be divided by the channel gain at the frequency of the respective tone. The result will be the frequency domain equalized vector $\mathbf{y}_{\text{f,e}} = \mathbf{x}_{\text{gfdm,f}} + \mathbf{v}_{\text{f}}$, where $\mathbf{x}_{\text{gfdm,f}}$ and $\mathbf{v}_{\text{f}}$ are the FFTs of $\mathbf{x}_{\text{gfdm}}$ and the channel noise vector **v**, respectively.

The procedure presented in [28] is a computationally efficient method for extracting the data symbols from $\mathbf{y}_{\text{f,e}}$. This procedure works as follows. The portion of the $\mathbf{y}_{\text{f,e}}$ that corresponds to each subcarrier is extracted through a frequency domain filtering; by applying a frequency mask. The extracted portion is shifted to the baseband and converted from the frequency domain to the time domain through an IFFT (of size M). The results for the kth subcarrier band are the estimates of transmitted data symbols $s_k[0], s_k[1], \ldots, s_k[M-1]$. A point that needs our attention here is that these estimates, even in the absence of channel noise, are not perfect. Because of the overlapping of the adjacent subcarrier filters in GFDM (see Fig. 3), the estimates are subject to ICI among adjacent subcarriers. This point has been acknowledged in [28] and an iterative method for successive interference cancellation (SIC) of ICI has been proposed. The successive ICI cancellation clearly has some drawbacks that put GFDM in a disadvantage when compared with C-FBMC that is introduced in a later part of this article.

In [28] it has also been noted that the iterative ICI cancellation may be avoided through a single step zero-forcing (ZF) or minimum mean-squared error (MMSE) solution which follows by noting that the transmit vector $\mathbf{x}_{\text{gfdm}}$ is related to the vector $\mathbf{s}_{\text{gfdm}} = [\mathbf{s}^{\text{T}}[0]\ \mathbf{s}^{\text{T}}[1]\ \cdots\ \mathbf{s}^{\text{T}}[M-1]]^{\text{T}}$ of all the transmitted symbols within the packet as

$$\mathbf{x}_{\text{gfdm}} = \mathbf{A}\mathbf{s}_{\text{gfdm}} \tag{16}$$

where **A** is a non-singular matrix that is determined by the packet parameters; see [26], [28] for details. Also, see [27] for the necessary condition for **A** not to be a singular matrix. One point that should be quoted from [27] is that for **A** to

be non-singular, M has to be an odd integer. Hence, the ZF detector that is presented below is strictly applicable to the cases where M is odd. The MMSE detector should also be applied to the cases where M is odd, as when M is even the receiver will suffer from a large level of noise enhancement.

The channel clearly has some impact. The received vector after stripping CP from it has the following form

$$\mathbf{y} = \mathbf{H}\mathbf{A}\mathbf{s}_{\text{gfdm}} + \mathbf{v} \tag{17}$$

where $\mathbf{H}$ is a circular matrix arising from the channel impulse response and $\mathbf{v}$ is the channel additive noise vector.

The ZF solution to (17) is thus obtained as

$$\mathbf{s}_{\text{gfdm}}^{\text{zf}} = (\mathbf{H}\mathbf{A})^{-1}\mathbf{y}. \tag{18}$$

On the other hand, the MMSE solution to (17) is calculated as

$$\mathbf{s}_{\text{gfdm}}^{\text{mmse}} = \left(\mathbf{R}_{vv} + \mathbf{A}^{\text{H}}\mathbf{H}^{\text{H}}\mathbf{H}\mathbf{A}\right)^{-1}\mathbf{A}^{\text{H}}\mathbf{H}^{\text{H}}\mathbf{y} \tag{19}$$

where $\mathbf{R}_{vv} = \text{E}[\mathbf{v}\mathbf{v}^{\text{H}}]$.

The direct solutions (18) and (19) may be prohibitive in complexity as the size of underlying matrices may be a few thousands in practice. Beside, as shown in [26] they both may incur some loss in performance, arising from some possible weak conditioning of $\mathbf{H}$ and/or $\mathbf{A}$. Taking note of these, the general consensus seem to be utilization of an SIC method [25]–[32]. Nevertheless, we note that recently algorithms that reduce the complexity of implementation of (18) and (19) have been proposed in [61] and [62].

D. Extension to MIMO Channels

The key idea that has made application of OFDM to MIMO channels trivial relies on the fact that each subcarrier signal is a pure tone (after removing the CP) and thus for each channel link it will be affected by a complex gain. For instance, if we consider a MIMO channel with N_{t} transmit antennas and N_{r} receive antennas that multiplexes N_{t} data streams in space, the equation relating an $N_{\text{t}} \times 1$ transmit data vector $\mathbf{s}_k$ of the kth subcarrier and the corresponding received signal vector (of size $N_{\text{r}} \times 1$) is obtained as

$$\mathbf{u}_k = \mathbf{H}_k\mathbf{s}_k + \mathbf{v}_k, \quad \text{for } k = 0, 1, \ldots, N-1 \tag{20}$$

where $\mathbf{u}_k$ is the received signal vector, $\mathbf{v}_k$ is the channel noise vector, and $\mathbf{H}_k$ is the channel gain matrix at the kth subcarrier frequency. Applying a ZF or MMSE equalizer to (20) will allow one to obtain an estimate of $\mathbf{s}_k$.

Noting that GFDM waveform is made up of MN tones, the same concept can be applied here too. An FFT of size MN is applied to the CP stripped received vector $\mathbf{y}$ of each received antenna and the results of the same indexed outputs are collected to obtain an equation similar to (20). Then, a ZF or MMSE equalizer is applied for each tone separately. This process gives estimates of the kth elements of the signal vector $\mathbf{x}_{\text{gfdm}}$ for all the space multiplexed signals. Collating the elements corresponding to each space multiplexed signal gives the estimate of the corresponding $\mathbf{x}_{\text{gfdm}}$ which then may be processed according to [28] to extract the respective data symbols.

For space-time coded (STC) transmission, particularly, the Alamouti codes [63], also one can benefit from the fact that each GFDM block is made of a summation of the tones and accordingly design an effective signaling scheme that benefit from the diversity gain provided by multiple antennas. Such a system has been developed and presented in [26]. The proposed method follows the time-reversal single-carrier approach that was first reported in [64] and later was adopted for FBMC systems (with linear convolution) in [65]. The method proposed in [26], for a MIMO setup with $N_{\text{t}} = 2$ and $N_{\text{r}} = 1$, is implemented as follows. For other choices of N_{t} and N_{r}, following the same line of thoughts, the respective designs can be made straightforwardly.

The first antenna transmits a block of GFDM that is characterized by the frequency domain vector $\mathbf{x}_{\text{gfdm,f,1}}$. Simultaneously, the second antenna transmits another block of GFDM that carries a different set of data symbols and is characterized by the frequency domain vector $\mathbf{x}_{\text{gfdm,f,2}}$. Next, both antennas transmit a second pair of GFDM blocks that are characterized by the frequency domain vectors $-\mathbf{x}_{\text{gfdm,f,2}}^{*}$ and $\mathbf{x}_{\text{gfdm,f,1}}^{*}$, transmitted from the first antenna and the second antenna, respectively. If the channel gains at the tones that form GFDM signal are presented by the diagonal matrices $\mathbf{H}_1$ and $\mathbf{H}_2$, the received signal blocks, after being CP stripped and passed through an FFT, result in

$$\mathbf{y}_1 = \mathbf{H}_1\mathbf{x}_{\text{gfdm,f,1}} + \mathbf{H}_2\mathbf{x}_{\text{gfdm,f,2}} + \mathbf{v}_1 \tag{21}$$

and

$$\mathbf{y}_2 = -\mathbf{H}_1\mathbf{x}_{\text{gfdm,f,2}}^{*} + \mathbf{H}_2\mathbf{x}_{\text{gfdm,f,1}}^{*} + \mathbf{v}_2, \tag{22}$$

for the first block and the second block, respectively. Using (21) and (22) and following the Alamouti method [64], estimates of $\mathbf{x}_{\text{gfdm,f,1}}$ and $\mathbf{x}_{\text{gfdm,f,2}}$ are calculated as

$$\begin{aligned}\hat{\mathbf{x}}_{\text{gfdm,f,1}} &= \left(\mathbf{H}_1\mathbf{H}_1^{*} + \mathbf{H}_2\mathbf{H}_2^{*}\right)^{-1}\left(\mathbf{H}_1^{*}\mathbf{y}_1 + \mathbf{H}_2\mathbf{y}_2^{*}\right)\\ &= \mathbf{x}_{\text{gfdm,f,1}}\\ &\quad + \left(\mathbf{H}_1\mathbf{H}_1^{*} + \mathbf{H}_2\mathbf{H}_2^{*}\right)^{-1}\left(\mathbf{H}_1^{*}\mathbf{v}_1 + \mathbf{H}_2\mathbf{v}_2^{*}\right)\end{aligned} \tag{23}$$

and

$$\begin{aligned}\hat{\mathbf{x}}_{\text{gfdm,f,2}} &= \left(\mathbf{H}_1\mathbf{H}_1^{*} + \mathbf{H}_2\mathbf{H}_2^{*}\right)^{-1}\left(\mathbf{H}_2^{*}\mathbf{y}_1 - \mathbf{H}_1\mathbf{y}_2^{*}\right)\\ &= \mathbf{x}_{\text{gfdm,f,2}}\\ &\quad + \left(\mathbf{H}_1\mathbf{H}_1^{*} + \mathbf{H}_2\mathbf{H}_2^{*}\right)^{-1}\left(\mathbf{H}_2^{*}\mathbf{v}_1 - \mathbf{H}_1\mathbf{v}_2^{*}\right),\end{aligned} \tag{24}$$

respectively. Once $\hat{\mathbf{x}}_{\text{gfdm,f,1}}$ and $\hat{\mathbf{x}}_{\text{gfdm,f,2}}$ are available, the method proposed in [28] may be used to extract the transmitted data symbols.

V. Circular FBMC

In this section, we show how the waveform construction that was developed in Section IV, for GFDM, can be also used to construct alternative waveforms based on FBMC signaling. To this end, we first present a short review of FBMC methods. These presentations follow the conventional FBMC systems where convolutions are linear. Extensions to GFDM-like waveforms, where linear convolutions are replaced by circular ones, will then follow. The prefix "C" is added whenever reference is made to the implementations that are based on circular convolution.

A. Historical Notes

Filter bank multicarrier (FBMC) methods were first proposed about 50 years ago, by Chang [66] and Saltzberg [67]. This was before the first introduction of OFDM in 1971 [68]. The method proposed by Chang considers transmission of a set of sequences of pulse amplitude modulated (PAM)/real-valued data symbols through a number of vestigial side-band (VSB) subcarriers. The subcarriers spectra are overlapped such that, following the Nyquist definition, a bandwidth efficiency of 100% is achieved. Saltzberg rearranged the real and imaginary parts of each symbol in a set of QAM symbol sequences such that they could be also transmitted with a bandwidth efficiency of 100%. Here, the real and imaginary parts of each QAM symbol are time staggered by half a symbol interval. In a recent work [69], we have shown that the methods presented in [66] and [67] are effectively the same and the names cosine modulated multitone (CMT) and staggered modulated multitone (SMT), respectively, have been suggested to refer to them.

Although SMT (often referred to as OQAM-OFDM) has been more popular in the literature, consideration of CMT for certain implementations may lead to more effective receivers. In particular, in some recent works [70], [71], we have shown that the blind equalization capability of CMT which has been introduced in [72] may prove very useful in overcoming the problem of pilot contamination (a serious problem [73]) in massive MIMO systems. Here, when it comes to the details of implementation of transmitter and receiver, we follow the norm in the literature and provide the details for SMT. Extensions to CMT are not much different and should be straightforward for an interested reader.

B. CMT

As noted above, in CMT data symbols are from a PAM alphabet. To establish a transmission with the maximum bandwidth efficiency, PAM symbols are distributed in a time-frequency phase-space lattice with a density of two symbols per unit area. This is equivalent to one complex symbol per unit area. Moreover, a 90 degree phase shift is introduced to the respective carriers among the adjacent symbols. These concepts are presented in Fig. 5. VSB modulation is applied to cope with the carrier spacing $F = 1/2T$. The pulse-shape used for this purpose at the transmitter as well as for matched filtering at the receiver is a square-root Nyquist waveform, $p(t)$, which has been designed such that $q(t) = p(t) \star p(-t)$ be a Nyquist pulse with regular zero crossings at $2T$ time intervals. Also, $p(t)$ by design is a real-valued even function of time, hence, $p(t) = p(-t)$. This implies that $P(f)$ is also a real-valued even function of the frequency.

Fig. 6 presents a set of magnitude responses of the modulated versions of the pulse-shape $p(t)$ for the data symbols transmitted at $t = 0$ and $t = T$. The colors used for the plots follow those in Fig. 5, to reflect the respective phase shifts.

C. SMT

SMT may be thought as an alternative to CMT [69]. Its time-frequency phase-space lattice is obtained from that of

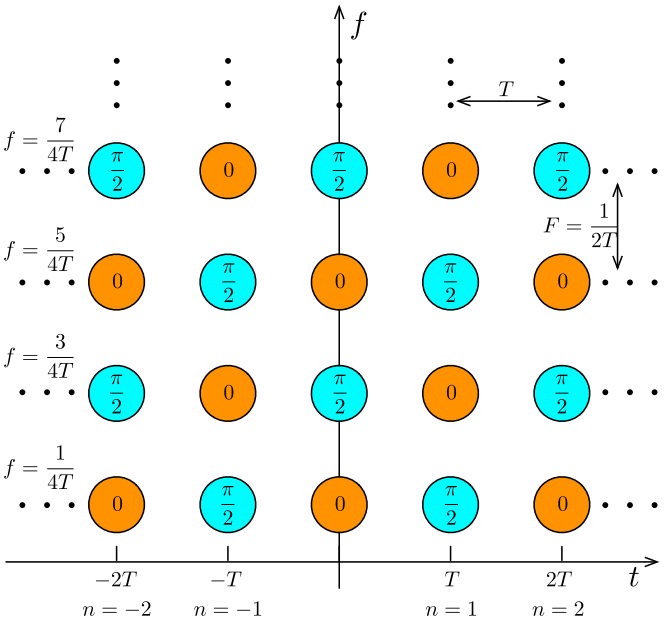

Fig. 5. The CMT time-frequency phase-space lattice. The circles show the position of data symbols and the content of each circle show the respective carrier phase.

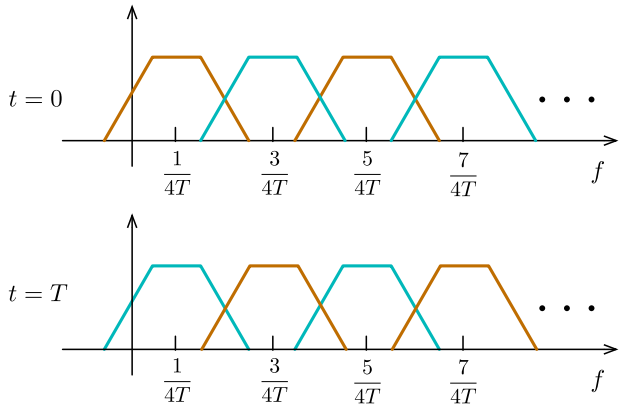

Fig. 6. Magnitude responses of the CMT pulse-shaping filters at various subcarriers and time instants $t = 0$ and $t = T$. The colors of the plots match those of the phase-space lattice points in Fig. 5 to remind us of the respective carrier phase angles.

CMT (Fig. 5) through a frequency shift of the lattice points down by $1/4T$, scaling the time axis by a factor $1/2$ and hence the frequency axis by a factor 2 [69]. This leads to the time-frequency phase-space lattice that is presented in Fig. 7. The magnitude responses of the SMT pulse-shaping filters at various subcarriers and time instants $t = 0$ and $t = T/2$ are presented in Fig. 8.

D. Transmitter Implementation

The transmitter implementation for both C-CMT and C-SMT follows the same procedure as GFDM. Minor changes are required to consider the phase adjustment of $\pi/2$ among adjacent symbols. Also, some adjustment to the width of subcarrier bands and their position have to be noted in the case of C-CMT. In C-SMT, on the other hand, it should be noted that in-phase and quadrature parts of QAM symbols have a

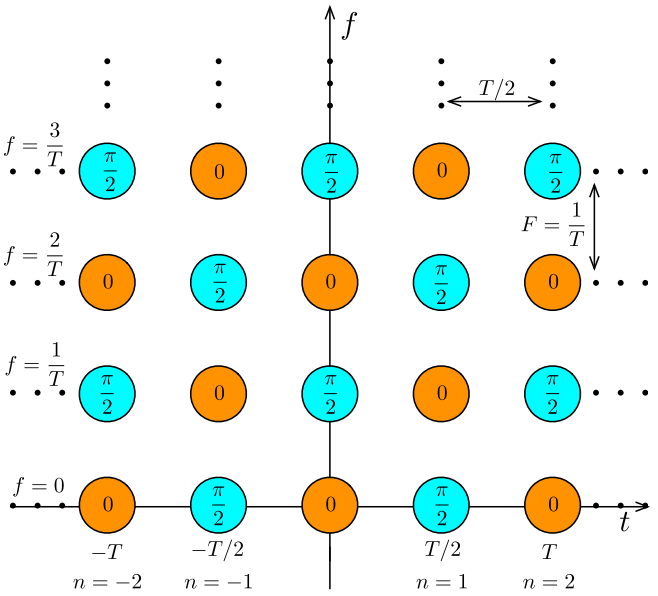

Fig. 7. The SMT time-frequency phase-space lattice. The circles show the position of data symbols and the content of each circle show the respective carrier phase angles.

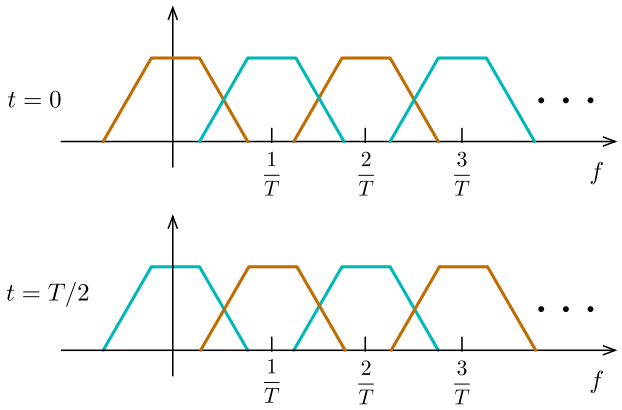

Fig. 8. Magnitude responses of the SMT pulse-shaping filters at various subcarriers and time instants $t = 0$ and $t = T/2$. The colors of the plots match those of the phase-space lattice points in Fig. 7 to remind us of the respective carrier phase angles.

time offset of $T/2$. In the rest of this section, we only discuss C-SMT and leave the C-CMT details for an interested reader to work out.

In C-SMT, a block/packet is constructed by taking the following steps:

1) For $m = 0, 1, \ldots, M-1$, let

$$\mathbf{s}_{\mathrm{R}}[n] = \left[s_{0,\mathrm{R}}[n]\ js_{1,\mathrm{R}}[n]\ \cdots\ j^{N-1}s_{N-1,\mathrm{R}}[n]\right]^{\mathrm{T}}$$

and

$$\mathbf{s}_{\mathrm{I}}[m] = \left[s_{0,\mathrm{I}}[n]\ js_{1,\mathrm{I}}[n]\ \cdots\ j^{N-1}s_{N-1,\mathrm{I}}[n]\right]^{\mathrm{T}}.$$

2) Construct the length MN vectors $\mathbf{x}_{\mathrm{R}}[n] = \mathbf{p} \odot (\mathcal{F}_{MN}^{-1}\mathbf{s}_{\mathrm{R,e}}[n])$ and $\mathbf{x}_{\mathrm{I}}[n] = \mathbf{p} \odot (\mathcal{F}_{MN}^{-1}\mathbf{s}_{\mathrm{I,e}}[n])$, where $\mathbf{s}_{\mathrm{R,e}}[n]$ and $\mathbf{s}_{\mathrm{I,e}}[n]$ are the M-fold expanded versions of $\mathbf{s}_{\mathrm{R}}[n]$ and $\mathbf{s}_{\mathrm{I}}[n]$, respectively.

3) Compute

$$\mathbf{x}_{\text{c-smt}} = \sum_{n=0}^{M-1} \mathrm{circshift}(\mathbf{x}_{\mathrm{R}}[n], nN) + j\sum_{n=0}^{M-1} \mathrm{circshift}(\mathbf{x}_{\mathrm{I}}[n], nN + N/2) \quad (25)$$

4) Add a CP to $\mathbf{x}_{\text{c-smt}}$

Note that in Step 2) $\mathcal{F}_{MN}^{-1}\mathbf{s}_{\mathrm{R,e}}[n]$ and $\mathcal{F}_{MN}^{-1}\mathbf{s}_{\mathrm{I,e}}[n]$ can be obtained efficiently by stacking M copies of the vectors $\mathcal{F}_N^{-1}\mathbf{s}_{\mathrm{R}}[n]$ and $\mathcal{F}_N^{-1}\mathbf{s}_{\mathrm{I}}[n]$, respectively, at the top of each other. Moreover, further reduction in complexity is possible by removing the factors of j in $\mathbf{s}_{\mathrm{R}}[n]$ and $\mathbf{s}_{\mathrm{I}}[n]$, calling the results $\tilde{\mathbf{s}}_{\mathrm{R}}[n]$ and $\tilde{\mathbf{s}}_{\mathrm{I}}[n]$, calculating $\mathcal{F}_N^{-1}\tilde{\mathbf{s}}_{\mathrm{R}}[n]$ and $\mathcal{F}_N^{-1}\tilde{\mathbf{s}}_{\mathrm{I}}[n]$, and cyclicly shifting the result by $N/4$ samples, to get $\mathcal{F}_N^{-1}\mathbf{s}_{\mathrm{R}}[n]$ and $\mathcal{F}_N^{-1}\mathbf{s}_{\mathrm{I}}[n]$, respectively. This procedure simplifies the calculations since the FFT of the pair of real vectors $\tilde{\mathbf{s}}_{\mathrm{R}}[n]$ and $\tilde{\mathbf{s}}_{\mathrm{I}}[n]$ can be performed with a complexity that is approximately equal to that of one FFT with a complex input [60]. This procedure has a complexity that is comparable to its GFDM counterpart. Also, this implementation has some similarity with the one presented in [34] and [36], however, these works did not mention the simplification steps that are noted here.

To further reveal the similarities of GFDM and C-SMT, we note that each C-SMT block is built based on the structure presented in Fig. 9. This should be compared with its GFDM counterpart in Fig. 2. Here, the data part of the block consists of $2M$ columns; M for the real parts and M for the imaginary parts of the data symbols. However, the total length of the block remains the same since, here, the successive columns are spaced by $T/2$. For the purpose of the C-SMT waveform construction, these columns are taken one at a time and the corresponding symbol vectors $\mathbf{s}_{\mathrm{R}}[n]$ and $\mathbf{s}_{\mathrm{I}}[n]$ are constructed. The results are then passed through an FFT block and expanded to the size MN. The pulse-shaping $\mathbf{p}$ is then applied and additional factor j is added if the input to the FFT is $\mathbf{s}_{\mathrm{I}}[n]$. Next, a circular shift of $N/2$ samples is applied to the accumulator before the accumulation step. This procedure leads to the C-SMT transmitter block diagram that is presented in Fig. 10. As seen, this block diagram, within couple of minor differences, is similar to its GFDM counterpart in Fig. 4.

E. Receiver Implementation

The receiver implementation in C-FBMC systems can also follow the steps mentioned in Section IV-C. Here, as opposed to GFDM, the embedded data symbols in $\mathbf{y}_{\mathrm{f,e}}$ are carried by a set of bases functions that are orthogonal with one another, where orthogonality is the *real orthogonality* defined in the FBMC literature see [19], [20], [74]. This, in turn, implies that the procedures mentioned in the second paragraph of Section IV-C will result in perfect recovery of data symbols, free of intersymbol interference (ISI) and ICI. In other words, here, no SIC is required.

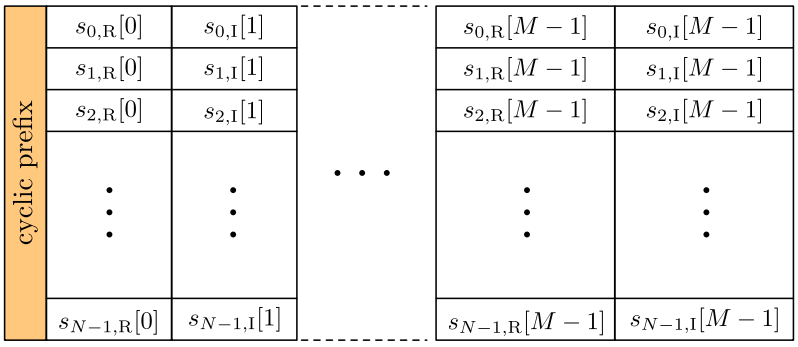

Fig. 9. A C-SMT block/packet.

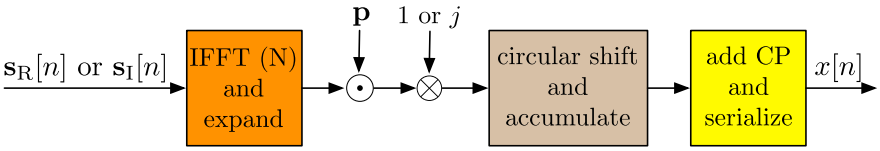

Fig. 10. A simplified implementation of C-SMT transmitter.

F. Extension to MIMO Channels

C-FBMC extension to MIMO channels is not different from that of GFDM. ZF or MMSE equalizer is applied in the frequency domain to separate the tones' amplitudes that correspond to different spatial sequences. Subsequently, the data extraction for each spatial stream is carried out separately according to the procedure that was discussed in the previous subsection. Alamouti STC can also be applied to C-FBMC following a similar procedure to the one discussed in [26] for GFDM. Detailed implementation of the Alamouti STC in C-FBMC has been reported in [75].

VI. UF-OFDM

A. Transmitter Implementation

Fig. 11 presents a block diagram of the UF-OFDM transmitter. A set of data symbols that corresponds to a given allocation of a single user are modulated over the assigned subcarriers through an IFFT processing block. The unused (zero) inputs to the IFFT block in Fig. 11 are reserved for other users in the network. The IFFT output is serialized and passed through a bandpass filter before transmission. The bandpass filter removes the OOB emissions that arise due to truncation of data carrying tones to the length of IFFT. By taking this filtering step, we are assured that different users in the network remain (approximately) orthogonal even under the conditions that they are not perfectly synchronized.

Unlike OFDM (as well as GFDM and C-FBMC), UF-OFDM does not rely on a CP to absorb the channel transient response. Instead, the output samples of IFFT are padded with a number of zeros equal to the duration of the impulse response of the bandpass filter. Moreover, the bandpass filter is designed such that the duration of its impulse response be equal to the common CP length used in OFDM [53]–[57]. This choice, although not necessary, equalizes the length of UF-OFDM and (CP-)OFDM symbols, hence, makes any comparison between the two straightforward.

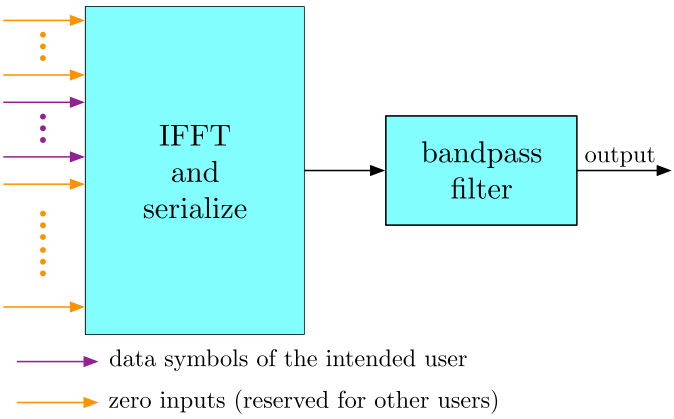

Fig. 11. Block diagram of a UF-OFDM transmitter.

For the discussions that follow, we let the size of IFFT in Fig. 11 be N, and assume the duration of the impulse response of the bandpass filter be equal to $N' + 1$, where $N' = N_{\mathrm{CP}}$ is the CP length in OFDM. Accordingly, each UF-OFDM symbol will have a length of $N + N'$. Following [53]–[57], we assume successive UF-OFDM symbols of this length are concatenated and transmitted, as in the case of OFDM.

B. Key Points

A few key points that help in understanding the main features of UF-OFDM are in order. First, we note that a UF-OFDM symbol that has been generated according to the procedure in Fig. 11, before going through the channel, preserves the orthogonality of the intended user's symbols perfectly. This fundamental point is the basis for the receiver structure that has been proposed in UF-OFDM literature [53]–[57] and is presented below. An explanation to this observation is provided in the next subsection. Second, the presence of channel expands the duration of each UF-OFDM symbol beyond the length of $N + N'$ samples. This concept is depicted in Fig. 12,

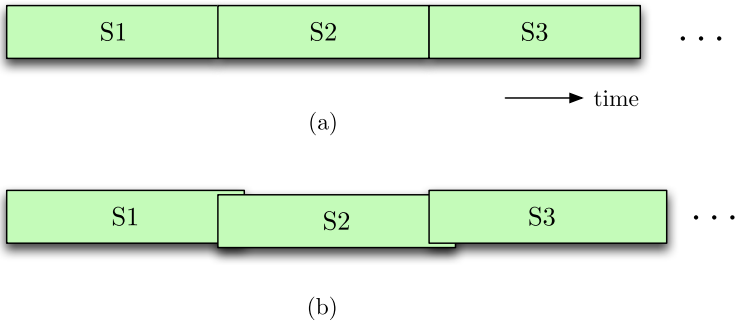

Fig. 12. A UF-OFDM symbol stream (a) before channel, and (b) after channel.

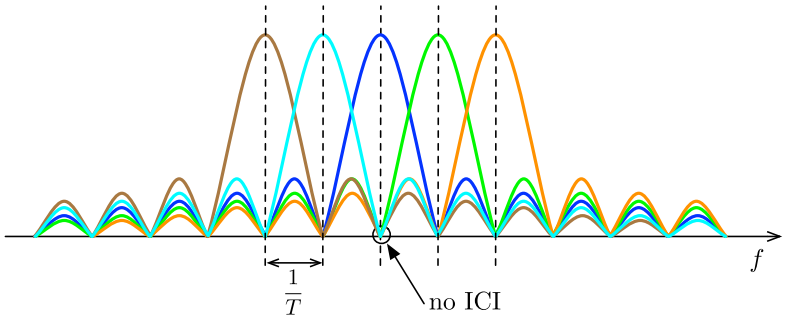

Fig. 13. Demonstration of the orthogonality of a set of tones that are time-limited to an interval T seconds and spaced by $1/T$ Hz.

where a stream of UF-OFDM symbols (S1, S2, $\cdots$) is depicted at the channel input and channel output. Obviously, channel introduces ISI among successive symbols. Also, if the processing at the receiver is made based on the segments of $N + N'$ samples of the received signal, some loss in the orthogonality of the intended user's data symbols will incur. By increasing the length of the segments, this loss of orthogonality can be recovered at the cost of an introduction of some ISI. It may be argued that although UF-OFDM has to be categorized as a non-orthogonal multicarrier system, the loss of orthogonality in many practical situations may remain insignificant. Thus, more often, UF-OFDM is categorized as a *quasi orthogonal signaling* method.

C. UF-OFDM Orthogonality

The IFFT output in Fig. 11 is the summation of a set of pure tones that is time limited to an interval T seconds (equivalently, N samples). We also recall that these tones are spaced in frequency by $1/T$ Hertz. In the frequency domain, these truncated tones are characterized by a set of sinc pulses, as depicted in Fig. 13. The orthogonality of the tones is characterized by the fact that they do not interfere with one another as along as they are sampled in the frequency domain at the middle of the sinc pulses; the vertical dashed lines in Fig. 13. The waveform duration T and the carrier/tone spacing $1/T$ guarantee this desirable orthogonality, as is well known in the OFDM literature.

Passing the summation of the tones through the bandpass filter at the UF-OFDM transmitter output attenuates the amplitude of the side-lobes that fall out of the band of interest, but, as depicted in Fig. 14, has no impact on the orthogonality of the subcarriers. This, clearly, shows that the filtering step in Fig. 11 does not affect the orthogonality of the subcarriers in UF-OFDM. The presence of channel, as demonstrated in Fig. 12, extends the length of each UF-OFDM symbol beyond $N + N'$ samples. Obviously, this also does not affect the orthogonality of the subcarriers and, hence, the data symbols can be recovered free of ICI if processing at the receiver is performed based on the extended length of the received signal samples. Nevertheless, as noted above, the detected symbols will suffer from ISI. One may choose to process a compromised length of the received signal samples to minimize the sum of ISI and ICI. One may also note that both ISI and ICI can be completely removed if the length of each UF-OFDM symbols is extended to $N + N'$ plus the maximum during of the channel impulse response by appending a set of zero samples at the end of each UF-OFDM symbol. This is equivalent to adding a guard interval in the time domain between the successive UF-OFDM symbols.

D. Filtering Options

Any bandpass filter that covers the subcarriers of the user of interest may be used. The proposers of UF-OFDM have emphasized on the use Dolph-Chebyshev filters [53], but have noted that other choices are also possible [54]. Methods to design filters that provide improved robustness to carrier frequency offset (CFO) and timing offset (TO) also have been reported [76].

Early works on the implementation of UF-OFDM assumed direct convolution of the IFFT output with a bandpass filter; as in Fig. 11. This implementation, which follows the principle of filtered OFDM, may be too complex as it requires about NN'

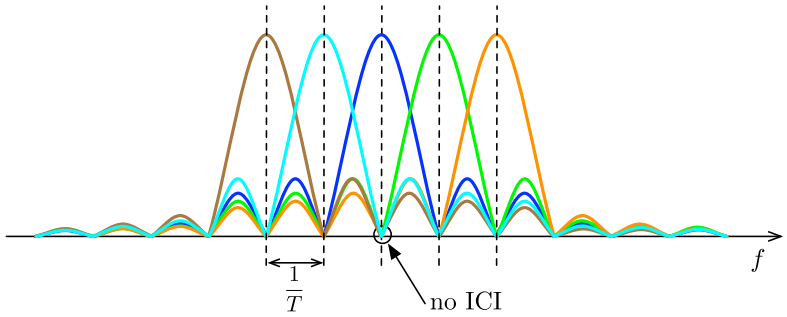

Fig. 14. The impact of the filtering in UF-OFDM on the spectra of subcarrier tones.

multiplications and additions. A recent result in [77] suggests a method of reducing this complexity significantly through a frequency domain implementation of the filtering operation. Another possibility that we suggest here is to apply a separate filter to each subcarrier as is done in the windowed OFDM, e.g., in IEEE 802.11a/g [78]. Here, all one needs to do is to apply a window with smooth roll-offs at the two sides to the IFFT output. It is equivalent to replacing the rectangular prototype filter in IFFT filter bank by a window with smooth transitions at the two sides. The advantage of this method is a very low complexity. It only requires $2N'$ multiplications. Nevertheless, it loses some flexibilities that direct filter design offers. A tutorial review of this method of filtering/windowing in OFDM and a method of optimizing the corresponding window function is available in [19].

E. Receiver Implementation

At the receiver side, the symbol boundaries are identified as part of the synchronization process. To recover the QAM data symbols carried in each UF-OFDM symbol, the respective segment of the received signal, usually consisting of $N + N'$ samples, is taken and appended with sufficient number of zeros to be extended to a vector of length $2N$. The result is then passed to an FFT block. The FFT outputs at the respective subcarriers (a set of odd or even indexed outputs) carry the desired symbol, scaled by channel gains at the respective frequencies. As in the conventional OFDM, the channel gains are compensated through a set of single tap equalizers; one per subcarrier.

We note that the above receiver structure that has been widely mentioned in the UF-OFDM literature [53]–[57] uses an FFT that has twice the length of the common FFT size in the conventional OFDM. Noting that only a decimated set of output samples of this extended length FFT are needed, one may argue that a time aliasing may be applied before applying the FFT. By doing so, an FFT of the same size as the conventional OFDM will be used. This point that has been missed in the UF-OFDM literature [53]–[57] has been previously adopted in the zipper discrete multitone (DMT) literature [79]–[82].

F. Extension to MIMO Channels

From the above discussions, we note that the presence of channel may result in the loss of orthogonality among the subcarriers. This potentially can limit the application of UF-OFDM in MIMO channels. However, since for channels with moderate spreading in time, the loss of orthogonality among subcarriers remains insignificant, MIMO processing techniques may be applied to separate subcarriers as in OFDM, albeit within some approximation. Such approximation may be avoided by adding a guard interval between the successive symbols of UF-OFDM. To emphasize, UF-OFDM can be used for both STC and MIMO space multiplexing with the same level of flexibility as OFDM. This follows from the fact that in UF-OFDM each data symbol modulates a single tone, as in OFDM.

VII. Multiuser Communications

As was noted earlier, the main motivation in proposing the new 5G waveforms is to reduce the interference among different users' signals when they are not perfectly synchronized. In this section, we make some comments on effectiveness of GFDM, C-FBMC, and UF-OFDM in handling multi-user signals when these signals may not be perfectly synchronized both in symbol timing and carrier frequency.

A. GFDM/C-FBMC

Fig. 15 depicts a communication scenario where a set of users are transmitting in an uplink of a network. The case presented is applicable to both GFDM and C-FBMC, but not to UF-OFDM. The case of UF-OFDM is discussed separately later. Each user transmits a sequence of GFDM/C-FBMC blocks. Each block has a structure similar to the one in Fig. 2. Each user channel introduces spreading in time to the respective GFDM/C-FBMC sequence and as a result the successive blocks may overlap. Also, with a relaxed synchronization among the users, the data blocks from different users may not be perfectly time aligned. Near perfect extraction of users' information may be achieved through a receiver signal processing algorithm as long as a *correct* time window of the received signal is chosen. A correct time window is the one that does not pick any user signal that suffers from blocks overlap. In Fig. 15, the time window B is a correct choice, but A and C both suffer from some inter-block interference. If the time window is selected incorrectly, the portions of the users' waveforms that belong to the transient parts will no longer be a sum of pure tones. Accordingly, the main features of GFDM/C-FBMC will not be preserved and the receiver signal

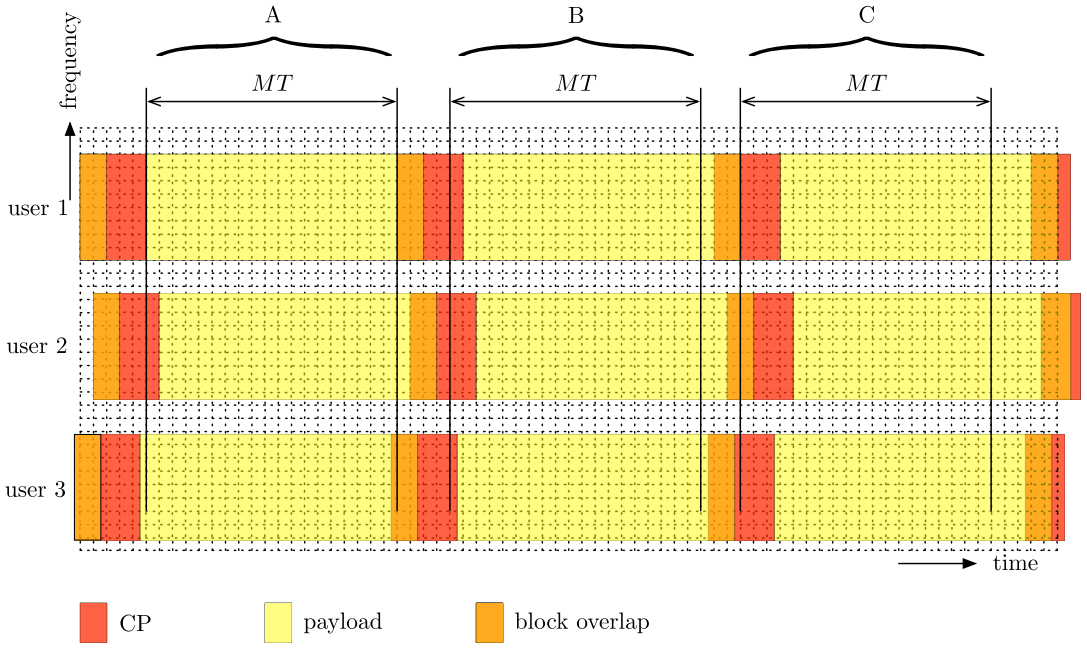

Fig. 15. A demonstration of a communication scenario where three users are transmitting simultaneously in uplink of a network. The users transmit over different frequency bands, but are not perfectly synchronized. This presentation is applicable to both GFDM and C-FBMC.

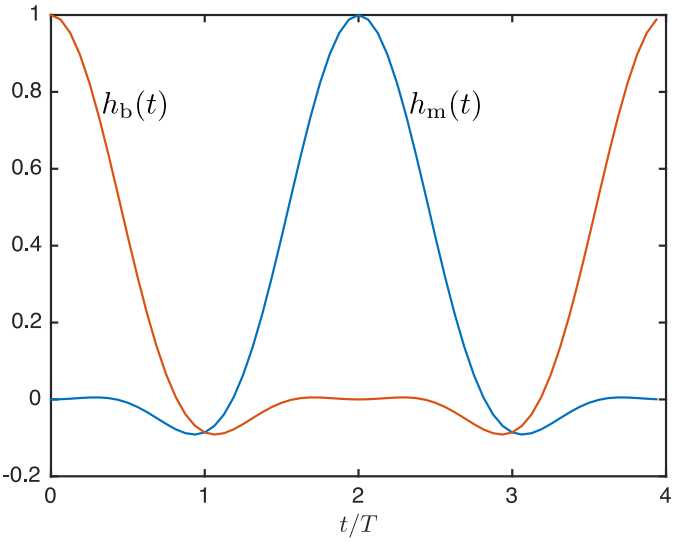

Fig. 16. Impulse responses of two samples of the prototype filter in a C-FBMC system for shaping the data symbols at the beginning of a packet (red) and the data symbols at the middle of the same packet (blue).

processing methods that were discussed in Sections IV and V will no longer work.

A correct choice of a window (of length MT) of the received signal that was discussed above avoids ISI, but cannot resolve the problem of inter-user interference, if the users are not perfectly carrier synchronized. Here, an attempt is made to clarify this point through couple of numerical examples without digging into the detailed mathematical equations. More on the subject of multi-user interference in GFDM and C-FBMC can be found in [83] and [84].

Fig. 16 presents two samples of the prototype filter in a GFDM/C-FBMC for the case where $N = 16$ and $M = 4$. These filters have been designed using the Matrin and Mirabbasi method [58], [59]. The prototype filter $h_{\rm b}(t)$ is for shaping the data symbols at the beginning of the packet, and $h_{\rm m}(t)$ is for shaping the data symbols at the middle of the packet. Similar filters are used at the receiver for matched filtering. We also recall that these prototype filters are modulated to the various subcarriers before being amplitude scaled by the respective data symbols.

Looking at the plots in Fig. 16, one may note that $h_{\rm m}(t)$ is a proper pulse shape as commonly seen in digital communication systems and $h_{\rm b}(t)$ is obtained by circularly shifting $h_{\rm m}(t)$ within the a window of length MT. This circular shift is an outcome of the circular convolutions in GFDM and C-FBMC. The magnitude of the Fourier transforms of $h_{\rm b}(t)$ and $h_{\rm m}(t)$ are presented in Fig. 17. Here, we note that while $H_{\rm m}(f)$ has a common lowpass response that we often see for pulse shaping filters, the magnitude response of $H_{\rm b}(f)$ is vastly different. However, $H_{\rm b}(f)$ and $H_{\rm m}(f)$ have the following common features. (i) $H_{\rm b}(0) = H_{\rm m}(0) = 1$. (ii) $H_{\rm b}(f)$ and $H_{\rm m}(f)$ share the same null frequencies. These null frequencies are at the positions $\frac{1}{T}$, $\frac{1}{T} + \frac{1}{MT}$, $\frac{1}{T} + \frac{2}{MT}$, $\cdots$. We also note that the less seen form of $H_{\rm b}(f)$, particularly its high side lobes beyond the point $fT = 1$, arises because of the sharp cut-offs (equivalently, discontinuities) at the beginning and the end of $h_{\rm b}(t)$.

Next, if we think of the modulated versions of $h_{\rm b}(t)$ and $h_{\rm m}(t)$ to the subcarriers center frequencies that are located at integer multiples of $\frac{1}{T}$, and recall that the sinusoidal tones synthesizing each subcarrier band are located at integer multiples of $\frac{1}{MT}$, one immediately finds that the position of the null points in $H_{\rm b}(f)$ and $H_{\rm m}(f)$ implies that in GFDM/C-FBMC any pair of non-adjacent subcarriers remain orthogonal

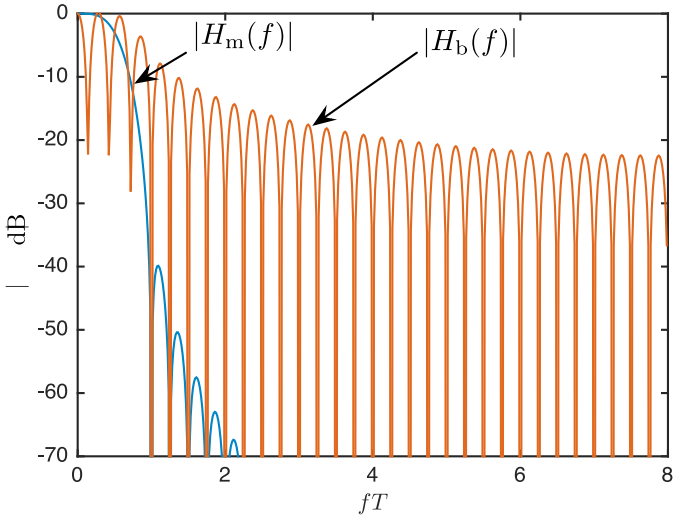

Fig. 17. Magnitude response of the prototype filters whose impulse responses are presented in Fig. 16.

to each others, if they are perfectly carrier synchronized. Clearly, if the pair of subcarriers are originated from the same transmitter/user, they will be synchronized and, thus, have no interference with one another. However, if they originate from different transmitters and, hence, there may be some mismatch between their respective carrier frequencies, multi-user interference can occur. For the data symbols at the middle of each packet such interference will remain insignificant, because of high attenuation in the stop-bands of the respective filters/pulse shapes. But for the data symbols at or near the beginning and the end of each packet, the level of interference can be significant because of poor responses of the respective filters.

Different measures can be taken to avoid multiuser interference in GFDM/C-FBMC. Among these, [84] has adopted the received signal windowing that was originally proposed in [79]–[82] and [85] to avoid out-of-band interference in DSL modems. This method requires an extension of the CP at the transmitter, and at the receiver a window of the received signal with a length larger than MT is used for signal processing and extraction of data symbols of different users. Interested readers are referred to [84] for the details.

The synthesized GDFM/C-FBMC waveforms also suffer from a poor OOB emissions, unless they are properly filtered at the transmitter output. This can be explained by making the following observation. Each GFDM or C-FBMC block (i.e., $\mathbf{x}_{\text{gfdm}}$ or $\mathbf{x}_{\text{c-fbmc}}$) is a summation of MN pure tones that are truncated to a length $T_{\text{cp}} + MT$. Truncation of each tone to the finite duration $T_{\text{cp}} + MT$ results in an equivalent 'sinc' spectrum with its well-known relatively large OOB emissions. Summing these spectra will lead to a spectrum with an undesirably large OOB emissions. To visualize this undesirable property of GDFM/C-FBMC waveforms (or circular waveforms, in general) we have presented in Figs. 18(a) and (b) sample spectra of GFDM and C-FBMC blocks. The block parameters here for both GFDM and C-FBMC are: $N = 128$, $M = 4$, and $N_{\text{cp}} = 32$. The number

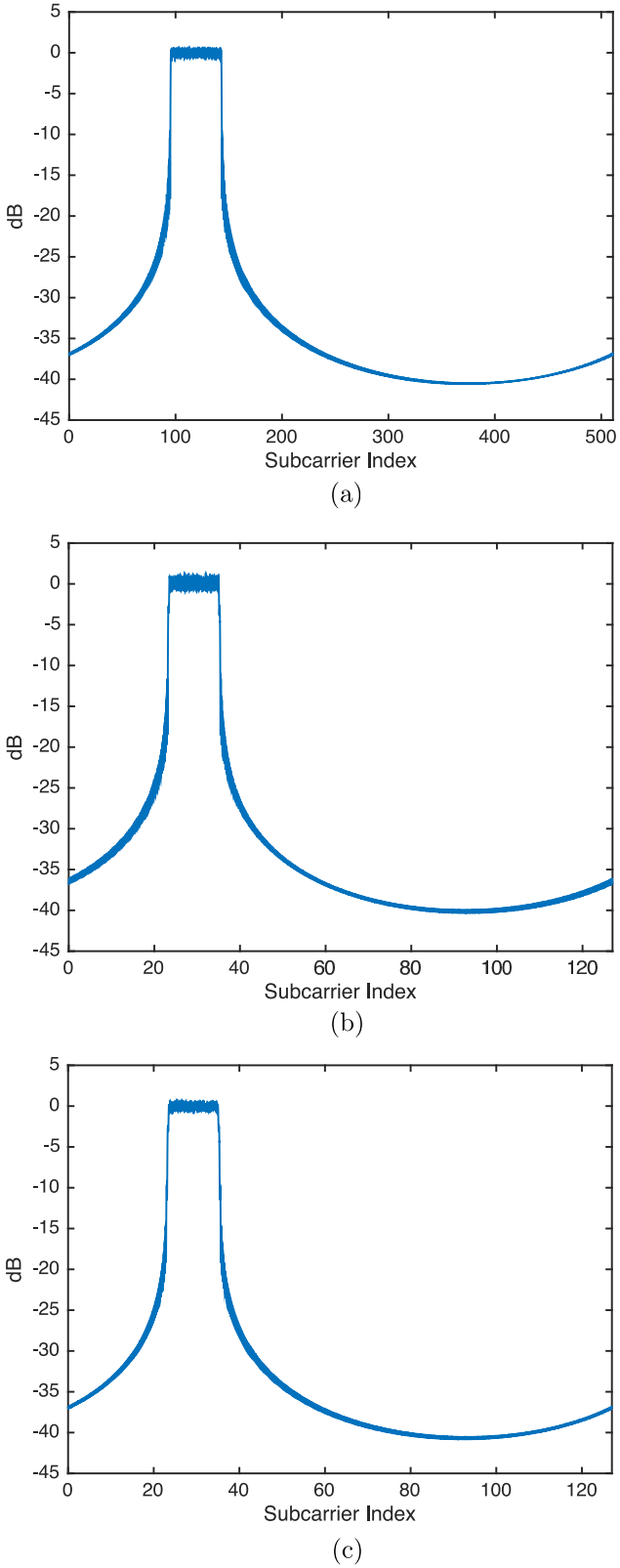

Fig. 18. An example of the power spectral densities of (a) GFDM, (b) C-FBMC, and (c) OFDM. The parameters are set so all three occupy the same frequency band and carry the same number of QAM data symbols. All are subject to a rectangular window for truncation to the specified length.

of active subcarriers is 12. For GFDM, the pulse-shaping filter is a square root raised-cosine with the roll-off factor $\alpha = 0.3$. For C-FBMC, the pulse-shaping filter is the PHYDYAS

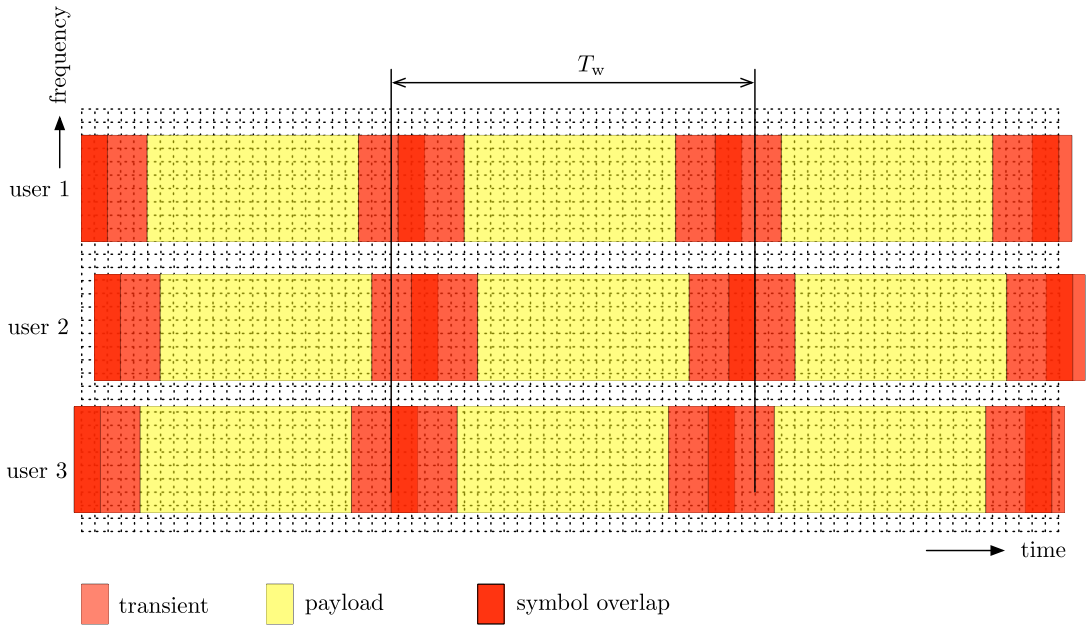

Fig. 19. A demonstration of a communication scenario where three users are transmitting simultaneously in uplink of a network. The users transmit over different frequency bands, but are not perfectly synchronized. This presentation is applicable to UF-OFDM.

prototype filter [22]; a widely accepted choice for FBMC applications.

To give an idea of how good/poor are these spectra, we have also presented in Fig. 18(c) the spectrum of an OFDM symbol with the IFFT length $MN = 512$ and $N_{\mathrm{cp}} = 32$. This equalizes the maximum number of tones based on which the three waveforms (GDFM, C-FBMC, and OFDM) are constructed. Moreover, to equalize the bandwidth of the generated waveforms, for OFDM we assume there are $12M = 48$ active subcarriers. The results presented in Fig. 18 are based on averaging the spectra of 100 independently generated blocks for each of the three waveforms. As seen, there is no noticeable difference between the three spectra. This means circular waveforms, no matter how good their prototype filter is designed, cannot offer any OOB emissions suppression better than OFDM. Hence, similar windowing and filtering methods that have been used to control the OOB emissions of OFDM have to be used for the circular waveforms as well. This observation seems to imply that the widely advertised statement that *circular waveforms solve the OOB emissions problem of OFDM and allow us to relax on perfect synchronization of different users in a network* is not accurate.

Finally, we may conclude from the above discussion that, as in OFDM, some sort of filtering has to be also applied to circular waveforms to resolve the problem of multiuser interference. Among various filtering methods that have been suggested for OFDM, UF-OFDM is the most recently proposed one and seems to be one of the top choices for 5G. The concept behind UF-OFDM may also be applied to the circular waveforms to introduce the class of UF-GFDM and UF-C-FBMC waveforms. These waveform will have the excellent filtering performance of UF-OFDM, and at the same time robust behavior of the circular waveforms to CFO differences in multi-users. A study of this of this combination of circular waveforms and the filtering operation behind UF-OFDM may thus prove useful and should be left for the future.

B. UF-OFDM

Fig. 19 presents a similar scenario to that of Fig. 15, for the case where transmission is based on UF-OFDM. Each UF-OFDM symbol has a transient at the beginning and a transient at the end. Each transient has a duration that is equal to the sum of the durations of the channel impulse response and the impulse response of the bandpass filter that is used at the transmitter to contain each user signal within the desired bandwidth, as well as any other processing in the transmitter/receiver chain. Here, the choice of the time window should include the transients on both sides of each UF-OFDM symbol, for all the users, to benefit from filtering operations that have been applied to resolve multi-user interference. Also, complete coverage of the transients assures the orthogonality of subcarriers for each user. However, as also noted earlier, an extended time window has the drawback of introducing ISI. Hence, in practice, a balanced decision has to be made on the size of the time window. The presented time window T_{w}, in Fig. 19, covers the transient periods of the middle symbol for the three users. However, because of the time misalignments of the users, this choice results in extra ISI from the adjacent symbols beyond the transients of the individual users. As noted earlier, by adding guard intervals between successive UF-OFDM symbols, ISI can be avoided at a cost of some reduction in spectral efficiency. The last point that should be mention here is the following. In a multiuser receiver that

receives signals from a number of users with unsynchronized carriers, a bank of filters has to be used at the receiver to avoid inter-user interference. This addition to UF-OFDM has been discussed in [86].

VIII. Conclusion

In this article, we presented a novel point of view of GFDM and C-FBMC modulation techniques; two new candidate waveforms of the upcoming fifth generation (5G) of wireless communication systems. We showed both GFDM and C-FBMC waveforms can be synthesized based on the same principle that OFDM waveform is built. The constructed waveforms can be viewed as a summation of a number of tones that at the receiver can be separated through application of an FFT. A number of lessons were learnt from this point of view:

1) Single tap per tone equalization can be applied as in OFDM.
2) Per tone MIMO equalization can be applied as in OFDM.
3) In terms of power spectral density and hence OOB emissions, GFDM/C-FBMC waveforms have no advantage over OFDM. Hence, filtering and windowing methods that have been applied to control OOB emissions in OFDM also should be adopted in GFDM and C-FBMC.

Moreover, we reviewed UF-OFDM, the third candidate waveform that has recently been proposed for 5G, and showed that this waveform also preserves the key features of OFDM.

The application of GFDM/C-FBMC and UF-OFDM to multiuser networks was also discussed briefly. It was noted that the variety of the receiver signal processing that have been applied to OFDM may be also used to avoid multiuser interference in GFDM/C-FBMC. UF-OFDM was found to be more relaxed to such needs.

Another point which was emphasized in this article was the fact that the non-orthogonality of GFDM is a disadvantage and, thus, makes this waveform less attractive than C-FBMC and UF-OFDM. However, more research is needed to weigh the advantages and disadvantages of C-FBMC and UF-OFDM as progress is being made in their development for 5G applications.

References

[1] W. Y. Chen, *DSL: Simulation Techniques and Standards Development for Digital Subscriber Line Systems*. Indianapolis, IN, USA: Macmillan Tech., 1998.

[2] T. Starr, J. M. Cioffi, and P. Silverman, *Understanding Digital Subscriber Line Technology*. Upper Saddle River, NJ, USA: Prentice Hall, 1999.

[3] R. V. Nee and R. Prasad, *OFDM for Wireless Multimedia Communications*. Boston, MA, USA: Artech House, 2000.

[4] Y. Li and G. Stüber, Eds., *Orthogonal Frequency Division Multiplexing for Wireless Communications*. Boston, MA, USA: Springer, 2006.

[5] M. Morelli, C.-C. J. Kuo, and M.-O. Pun, "Synchronization techniques for orthogonal frequency division multiple access (OFDMA): A tutorial review," *Proc. IEEE*, vol. 95, no. 7, pp. 1394–1427, Jul. 2007.

[6] D. Huang and K. B. Letaief, "An interference-cancellation scheme for carrier frequency offsets correction in OFDMA systems," *IEEE Trans. Commun.*, vol. 53, no. 7, pp. 1155–1165, Jul. 2005.

[7] K. Lee and I. Lee, "CFO compensation for uplink OFDMA systems with conjugated gradient," in *Proc. IEEE ICC*, Kyoto, Japan, Jun. 2011, pp. 1–5.

[8] K. Lee, S.-R. Lee, S.-H. Moon, and I. Lee, "MMSE-based CFO compensation for uplink OFDMA systems with conjugate gradient," *IEEE Trans. Wireless Commun.*, vol. 11, no. 8, pp. 2767–2775, Aug. 2012.

[9] A. Farhang, N. Marchetti, and L. E. Doyle, "Low complexity LS and MMSE based CFO compensation techniques for the uplink of OFDMA systems," in *Proc. IEEE Int. Conf. Commun. (ICC)*, Budapest, Hungary, 2013, pp. 5748–5753.

[10] H. Saeedi-Sourck, Y. Wu, J. W. M. Bergmans, S. Sadri, and B. Farhang-Boroujeny, "Complexity and performance comparison of filter bank multicarrier and OFDM in uplink of multicarrier multiple access networks," *IEEE Trans. Signal Process.*, vol. 59, no. 4, pp. 1907–1912, Apr. 2011.

[11] S. Brandes, I. Cosovic, and M. Schnell, "Sidelobe suppression in OFDM systems by insertion of cancellation carriers," in *Proc. IEEE 62nd Veh. Technol. Conf. (VTC)*, vol. 1. Dallas, TX, USA, 2005, pp. 152–156.

[12] Z. Yuan, S. Pagadarai, and A. M. Wyglinski, "Cancellation carrier technique using genetic algorithm for OFDM sidelobe suppression," in *Proc. IEEE Military Commun. Conf. (MILCOM)*, San Diego, CA, USA, 2008, pp. 1–5.

[13] A. Selim, I. Macaluso, and L. Doyle, "Efficient sidelobe suppression for OFDM systems using advanced cancellation carriers," in *Proc. IEEE Int. Conf. Commun. (ICC)*, Budapest, Hungary, 2013, pp. 4687–4692.

[14] S. N. Premnath, D. Wasden, S. K. Kasera, B. Farhang-Boroujeny, and N. Patwari, "Beyond OFDM: Best-effort dynamic spectrum access using filterbank multicarrier," in *Proc. 4th Int. Conf. Commun. Syst. Netw. (COMSNETS)*, Bengaluru, India, 2012, pp. 1–10.

[15] S. N. Premnath, D. Wasden, S. Kasera, N. Patwari, and B. Farhang-Boroujeny, "Beyond OFDM: Best-effort dynamic spectrum access using filterbank multicarrier," *IEEE/ACM Trans. Netw.*, vol. 21, no. 3, pp. 869–882, Jun. 2013.

[16] B. Farhang-Boroujeny and R. Kempter, "Multicarrier communication techniques for spectrum sensing and communication in cognitive radios," *IEEE Commun. Mag.*, vol. 46, no. 4, pp. 80–85, Apr. 2008.

[17] B. Farhang-Boroujeny, "Prolate filters for nonadaptive multitaper spectral estimators with high spectral dynamic range," *IEEE Signal Process. Lett.*, vol. 15, no. 5, pp. 457–460, May 2008.

[18] B. Farhang-Boroujeny, "Filter bank spectrum sensing for cognitive radios," *IEEE Trans. Signal Process.*, vol. 56, no. 5, pp. 1801–1811, May 2008.

[19] B. Farhang-Boroujeny, "OFDM versus filter bank multicarrier," *IEEE Signal Process. Mag.*, vol. 28, no. 3, pp. 92–112, May 2011.

[20] B. Farhang-Boroujeny, "Filter bank multicarrier modulation: A waveform candidate for 5G and beyond," *Adv. Elect. Eng.*, vol. 2014, Nov. 2014, Art. no. 482805.

[21] A. Sahin, I. Guvenc, and H. Arslan, "A survey on multicarrier communications: Prototype filters, lattice structures, and implementation aspects," *IEEE Commun. Surveys Tuts.*, vol. 16, no. 3, pp. 1312–1338, 3rd Quart. 2014.

[22] M. Bellanger, "FBMC physical layer: A primer," PHYDYAS, Paris, France, Tech. Rep., Jun. 2010. [Online]. Available: http://www.ict-phydyas.org/teamspace/internal-folder/FBMC-Primer_06-2010.pdf

[23] M. Payaró, A. Pascual-Iserte, and M. Najar, "Performance comparison between FBMC and OFDM in MIMO systems under channel uncertainty," in *Proc. Eur. Wireless Conf. (EW)*, Lucca, Italy, 2010, pp. 1023–1030.

[24] T. Ihalainen, A. Ikhlef, J. Louveaux, and M. Renfors, "Channel equalization for multi-antenna FBMC/OQAM receivers," *IEEE Trans. Veh. Technol.*, vol. 60, no. 5, pp. 2070–2085, Jun. 2011.

[25] G. Fettweis, M. Krondorf, and S. Bittner, "GFDM—Generalized frequency division multiplexing," in *Proc. IEEE 69th Veh. Technol. Conf. (VTC)*, Barcelona, Spain, Apr. 2009, pp. 1–4.

[26] N. Michailow *et al.*, "Generalized frequency division multiplexing for 5th generation cellular networks," *IEEE Trans. Commun.*, vol. 62, no. 9, pp. 3045–3061, Sep. 2014.

[27] M. Matthe, L. L. Mendes, and G. Fettweis, "Generalized frequency division multiplexing in a Gabor transform setting," *IEEE Commun. Lett.*, vol. 18, no. 8, pp. 1379–1382, Aug. 2014.

[28] I. Gaspar *et al.*, "Low complexity GFDM receiver based on sparse frequency domain processing," in *Proc. IEEE 77th Veh. Technol. Conf. (VTC)*, Dresden, Germany, Jun. 2013, pp. 1–6.

[29] M. Matthe, L. L. Mendes, and G. Fettweis, "Space-time coding for generalized frequency division multiplexing," in *Proc. 20th Eur. Wireless Conf.*, Barcelona, Spain, May 2014, pp. 1–5.

[30] N. Michailow, I. Gaspar, S. Krone, M. Lentmaier, and G. Fettweis, "Generalized frequency division multiplexing: Analysis of an alternative multi-carrier technique for next generation cellular systems," in *Proc. IEEE Int. Symp. Wireless Commun. Syst. (ISWCS)*, Paris, France, Aug. 2012, pp. 171–175.

[31] R. Datta, N. Michailow, S. Krone, M. Lentmaier, and G. Fettweis, "Generalized frequency division multiplexing in cognitive radio," in *Proc. IEEE Int. Symp. Wireless Commun. Syst. (ISWCS)*, Paris, France, Aug. 2012, pp. 2679–2683.

[32] M. Danneberg, R. Datta, A. Festag, and G. Fettweis, "Experimental testbed for 5G cognitive radio access in 4G LTE cellular systems," in *Proc. IEEE 8th Sensor Array Multichannel Signal Process. Workshop (SAM)*, A Coruña, Spain, Jun. 2014, pp. 321–324.

[33] M. J. Abdoli, M. Jia, and J. Ma, "Weighted circularly convolved filtering in OFDM/OQAM," in *Proc. IEEE 24th Int. Symp. Pers. Indoor Mobile Radio Commun. (PIMRC)*, London, U.K., Sep. 2013, pp. 657–661.

[34] H. Lin and P. Siohan, "An advanced multi-carrier modulation for future radio systems," in *Proc. IEEE Int. Conf. Acoust. Speech Signal Process. (ICASSP)*, Florence, Italy, May 2014, pp. 8097–8101.

[35] M. Schellmann *et al.*, "FBMC-based air interface for 5G mobile: Challenges and proposed solutions," in *Proc. 9th Int. Conf. Cogn. Radio Orient. Wireless Netw. Commun. (CROWNCOM)*, Oulu, Finland, Jun. 2014, pp. 102–107.

[36] H. Lin and P. Siohan, "Multi-carrier modulation analysis and WCP-COQAM proposal," *EURASIP J. Adv. Signal Process.*, vol. 2014, no. 1, pp. 1–19, 2014. [Online]. Available: http://dx.doi.org/10.1186/1687-6180-2014-79

[37] B. Farhang-Boroujeny and H. Moradi, "Derivation of GFDM based on OFDM principles," in *Proc. IEEE Int. Conf. Commun. (ICC)*, London, U.K., Jun. 2015, pp. 2680–2685.

[38] A. M. Tonello, "A novel multi-carrier scheme: Cyclic block filtered multitone modulation," in *Proc. IEEE Int. Conf. Commun. (ICC)*, Budapest, Hungary, Jun. 2013, pp. 5263–5267.

[39] A. M. Tonello and M. Girotto, "Cyclic block FMT modulation for communications in time-variant frequency selective fading channels," in *Proc. 21st Eur. Signal Process. Conf. (EUSIPCO)*, Sep. 2013, pp. 1–5.

[40] A. M. Tonello and M. Girotto, "Cyclic block FMT modulation for broadband power line communications," in *Proc. IEEE 17th Int. Symp. Power Line Commun. Appl. (ISPLC)*, Johannesburg, South Africa, Mar. 2013, pp. 247–251.

[41] H. G. Myung, J. Lim, and D. J. Goodman, "Single carrier FDMA for uplink wireless transmission," *IEEE Veh. Technol. Mag.*, vol. 1, no. 3, pp. 30–38, Sep. 2006.

[42] H. G. Myung, J. Lim, and D. J. Goodman, "Peak-to-average power ratio of single carrier FDMA signals with pulse shaping," in *Proc. IEEE 17th Int. Symp. Pers. Indoor Mobile Radio Commun.*, Helsinki, Finland, Sep. 2006, pp. 1–5.

[43] G. Berardinelli, F. M. L. Tavares, T. B. Sorensen, P. Mogensen, and K. Pajukoski, "Zero-tail DFT-spread-OFDM signals," in *Proc. IEEE Globecom Workshops (GC Wkshps)*, Atlanta, GA, USA, Dec. 2013, pp. 229–234.

[44] M. Huemer, C. Hofbauer, and J. B. Huber, "The potential of unique words in OFDM," in *Proc. 15th Int. OFDM-Workshop*, Hamburg, Germany, Sep. 2010, pp. 140–144.

[45] A. Onic and M. Huemer, "Direct versus two-step approach for unique word generation in UW-OFDM," in *Proc. 15th Int. OFDM-Workshop*, Hamburg, Germany, Sep. 2010, pp. 145–149.

[46] M. Huemer, A. Onic, and C. Hofbauer, "Classical and Bayesian linear data estimators for unique word OFDM," *IEEE Trans. Signal Process.*, vol. 59, no. 12, pp. 6073–6085, Dec. 2011.

[47] B. Muquet, M. de Courville, G. B. Giannakis, Z. Wang, and P. Duhamel, "Reduced complexity equalizers for zero-padded OFDM transmissions," in *Proc. IEEE Int. Conf. Acoust. Speech Signal Process. (ICASSP)*, vol. 5. Istanbul, Turkey, May 2000, pp. 2973–2976.

[48] Z. Wang, X. Ma, and G. B. Giannakis, "Optimality of single-carrier zero-padded block transmissions," in *Proc. IEEE Wireless Commun. Netw. Conf. (WCNC)*, vol. 2. Orlando, FL, USA, Mar. 2002, pp. 660–664.

[49] S. Tang *et al.*, "Iterative channel estimation for block transmission with known symbol padding—A new look at TDS-OFDM," in *Proc. IEEE Global Telecommun. Conf. (GLOBECOM)*, Washington, DC, USA, Nov. 2007, pp. 4269–4273.

[50] D. V. Welden and H. Steendam, "Iterative EM based channel estimation for KSP-OFDM," in *Proc. IEEE 19th Int. Symp. Pers. Indoor Mobile Radio Commun. (PIMRC)*, Cannes, France, Sep. 2008, pp. 1–5.

[51] D. V. Welden, H. Steendam, and M. Moeneclaey, "Iterative DA/DD channel estimation for KSP-OFDM," in *Proc. IEEE Int. Conf. Commun. (ICC)*, Beijing, China, May 2008, pp. 693–697.

[52] D. V. Welden and H. Steendam, "Near optimal iterative channel estimation for KSP-OFDM," *IEEE Trans. Signal Process.*, vol. 58, no. 9, pp. 4948–4954, Sep. 2010.

[53] V. Vakilian, T. Wild, F. Schaich, S. ten Brink, and J.-F. Frigon, "Universal-filtered multi-carrier technique for wireless systems beyond LTE," in *Proc. IEEE Globecom Workshops (GC Wkshps)*, Atlanta, GA, USA, Dec. 2013, pp. 223–228.

[54] X. Wang, T. Wild, F. Schaich, and A. F. dos Santos, "Universal filtered multi-carrier with leakage-based filter optimization," in *Proc. 20th Eur. Wireless Conf.*, Barcelona, Spain, May 2014, pp. 1–5.

[55] T. Wild, F. Schaich, and Y. Chen, "5G air interface design based on universal filtered (UF-)OFDM," in *Proc. 19th Int. Conf. Digit. Signal Process. (DSP)*, Hong Kong, Aug. 2014, pp. 699–704.

[56] F. Schaich and T. Wild, "Waveform contenders for 5G—OFDM vs. FBMC vs. UFMC," in *Proc. 6th Int. Symp. Commun. Control Signal Process. (ISCCSP)*, Athens, Greece, May 2014, pp. 457–460.

[57] F. Schaich and T. Wild, "Relaxed synchronization support of universal filtered multi-carrier including autonomous timing advance," in *Proc. 11th Int. Symp. Wireless Commun. Syst. (ISWCS)*, Barcelona, Spain, Aug. 2014, pp. 203–208.

[58] K. W. Martin, "Small side-lobe filter design for multitone data-communication applications," *IEEE Trans. Circuits Syst. II, Analog Digit. Signal Process.*, vol. 45, no. 8, pp. 1155–1161, Aug. 1998.

[59] S. Mirabbasi and K. Martin, "Overlapped complex-modulated transmultiplexer filters with simplified design and superior stopbands," *IEEE Trans. Circuits Syst. II, Analog Digit. Signal Process.*, vol. 50, no. 8, pp. 456–469, Aug. 2003.

[60] A. V. Oppenheim and R. W. Schafer, *Digital Signal Processing*. Englewood Cliffs, NJ, USA: Prentice-Hall, 1975.

[61] A. Farhang, N. Marchetti, and L. E. Doyle, "Low complexity GFDM receiver design: A new approach," in *Proc. IEEE Int. Conf. Commun. (ICC)*, London, U.K., Jun. 2015, pp. 4775–4780.

[62] A. Farhang, N. Marchetti, and L. E. Doyle, "Low-complexity modem design for GFDM," *IEEE Trans. Signal Process.*, vol. 64, no. 6, pp. 1507–1518, Mar. 2016.

[63] S. M. Alamouti, "A simple transmit diversity technique for wireless communications," *IEEE J. Sel. Areas Commun.*, vol. 16, no. 8, pp. 1451–1458, Oct. 1998.

[64] N. Al-Dhahir, "Single-carrier frequency-domain equalization for space-time block-coded transmissions over frequency-selective fading channels," *IEEE Commun. Lett.*, vol. 5, no. 7, pp. 304–306, Jul. 2001.

[65] M. Renfors, T. Ihalainen, and T. H. Stitz, "A block-Alamouti scheme for filter bank based multicarrier transmission," in *Proc. Eur. Wireless Conf. (EW)*, Lucca, Italy, Apr. 2010, pp. 1031–1037.

[66] R. W. Chang, "Synthesis of band-limited orthogonal signals for multichannel data transmission," *Bell Sys. Tech. J.*, vol. 45, no. 10, pp. 1775–1796, Dec. 1966.

[67] B. Saltzberg, "Performance of an efficient parallel data transmission system," *IEEE Trans. Commun. Technol.*, vol. 15, no. 6, pp. 805–811, Dec. 1967.

[68] S. B. Weinstein and P. M. Ebert, "Data transmission by frequency-division multiplexing using the discrete Fourier transform," *IEEE Trans. Commun. Technol.*, vol. 19, no. 5, pp. 628–634, Oct. 1971.

[69] B. Farhang-Boroujeny and C. Him (George) Yuen, "Cosine modulated and offset QAM filter bank multicarrier techniques: A continuous-time prospect," *EURASIP J. Adv. Signal Process.*, vol. 2010, 2010, Art. no. 165654.

[70] A. Farhang, N. Marchetti, L. E. Doyle, and B. Farhang-Boroujeny, "Filter bank multicarrier for massive MIMO," in *Proc. 80th Veh. Technol. Conf. (VTC Fall)*, Vancouver, BC, Canada, 2014, pp. 1–7.

[71] A. Farhang, A. Aminjavaheri, N. Marchetti, L. E. Doyle, and B. Farhang-Boroujeny, "Pilot decontamination in CMT-based massive MIMO networks," in *Proc. IEEE 11th Int. Symp. Wireless Commun. Syst. (ISWCS)*, Barcelona, Spain, Aug. 2014, pp. 589–593.

[72] B. Farhang-Boroujeny, "Multicarrier modulation with blind detection capability using cosine modulated filter banks," *IEEE Trans. Commun.*, vol. 51, no. 12, pp. 2057–2070, Dec. 2003.

[73] J. Jose, A. Ashikhmin, T. Marzetta, and S. Vishwanath, "Pilot contamination and precoding in multi-cell TDD systems," *IEEE Trans. Wireless Commun.*, vol. 10, no. 8, pp. 2640–2651, Aug. 2011.

[74] B. Le Floch, M. Alard, and C. Berrou, "Coded orthogonal frequency division multiplex," *Proc. IEEE*, vol. 83, no. 6, pp. 982–996, Jun. 1995.

[75] D. Kong, X.-G. Xia, and T. Jiang, *An Alamouti Coded CP-FBMC-MIMO System With Two Transmit Antennas*. Sci. China Press, Beijing, 2015, pp. 1–6. [Online]. Available: http://dx.doi.org/10.1007/s11432-015-5345-3

[76] X. Wang, T. Wild, and F. Schaich, "Filter optimization for carrier-frequency- and timing-offset in universal filtered multi-carrier systems," in *Proc. IEEE 81st Veh. Technol. Conf. (VTC Spring)*, Glasgow, U.K., May 2015, pp. 1–6.
[77] T. Wild and F. Schaich, "A reduced complexity transmitter for UF-OFDM," in *Proc. IEEE 81st Veh. Technol. Conf. (VTC Spring)*, Glasgow, U.K., May 2015, pp. 1–6.
[78] B. Farhang-Boroujeny, *Signal Processing Techniques for Software Radios*, 2nd ed. Stockholm, Sweden: Lulu Pub. House, 2009.
[79] F. Sjoberg, R. Nilsson, M. Isaksson, P. Odling, and P. O. Borjesson, "Asynchronous zipper," in *Proc. IEEE Int. Conf. Commun. (ICC)*, vol. 1. Vancouver, BC, Canada, May 1999, pp. 231–235.
[80] D. G. Mestdagh, M. R. Isaksson, and P. Odling, "Zipper VDSL: A solution for robust duplex communication over telephone lines," *IEEE Commun. Mag.*, vol. 38, no. 5, pp. 90–96, May 2000.
[81] M. D. Nava and G. S. Okvist, "The Zipper prototype: A complete and flexible VDSL multicarrier solution," *IEEE Commun. Mag.*, vol. 40, no. 12, pp. 92–105, Dec. 2002.
[82] R. Nilsson, F. Sjoberg, M. Isaksson, J. M. Cioffi, and S. K. Wilson, "Autonomous synchronization of a DMT-VDSL system in unbundled networks," *IEEE J. Sel. Areas Commun.*, vol. 20, no. 5, pp. 1055–1063, Jun. 2002.
[83] A. Aminjavaheri, A. Farhang, A. L. RezazadehReyhani, and B. Farhang-Boroujeny, "Impact of timing and frequency offsets on multicarrier waveform candidates for 5G," in *Proc. IEEE DSP Workshop Edu.*, Salt Lake City, UT, USA, Aug. 2015, pp. 178–183.
[84] A. L. RezazadehReyhani and B. Farhang-Boroujeny, "Asynchronous performance of circularly pulse-shaped waveforms for 5G," arXiv:1511.07910, 2016.
[85] "Very-high bit-rate digital subscriber lines (VDSL) metallic interface, part 3: Technical specification of a multi-carrier modulation transceiver," document T1E1.4/2000-013R3, Working Group R1E1.4, Savannah, GA, USA, Nov. 2000.
[86] J. Abdoli, M. Jia, and J. Ma, "Filtered OFDM: A new waveform for future wireless systems," in *Proc. IEEE 16th Int. Workshop Signal Process. Adv. Wireless Commun. (SPAWC)*, Stockholm, Sweden, Jun./Jul. 2015, pp. 66–70.

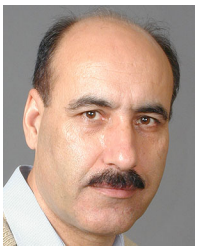

Behrouz Farhang-Boroujeny (M'84–SM'90) received the B.Sc. degree in electrical engineering from Teheran University, Iran, in 1976, the M.Eng. degree from University of Wales Institute of Science and Technology, U.K., in 1977, and the Ph.D. degree from Imperial College, University of London, U.K., in 1981. From 1981 to 1989, he was with the Isfahan University of Technology, Isfahan, Iran. From 1989 to 2000, he was with the National University of Singapore. Since August 2000, he has been with the University of Utah.

He is an expert in the general area of signal processing. His current scientific interests are adaptive filters, multicarrier communications, detection techniques for space-time coded systems, and cognitive radios. In the past, he has worked and has made significant contribution to areas of adaptive filters theory, acoustic echo cancellation, magnetic/optical recoding, and digital subscriber line technologies. He is the author of the books *Adaptive Filters: Theory and Applications* (2nd ed.; John Wiley & Sons, 1998, 2013) and *Signal Processing Techniques for Software Radios* (2nd ed.; self-published at Lulu Publishing House, 2009, 2010).

Dr. Farhang-Boroujeny received the UNESCO Regional Office of Science and Technology for South and Central Asia Young Scientists Award in 1987. He served as an Associate Editor of IEEE TRANSACTIONS ON SIGNAL PROCESSING from July 2002 to July 2005, and as an Associate Editor of IEEE SIGNAL PROCESSING LETTERS from April 2008 to March 2010. He has also been involved in various IEEE activities, including the chairmanship of the Signal Processing/Communications chapter of IEEE of Utah in 2004 and 2005.

Hussein Moradi received the bachelor's degree from University of Texas at Arlington, and the doctorate and master's degrees from Southern Methodist University, Dallas. He joined Idaho National Laboratory in November 2009 as Chief Wireless Scientist. He brings more than 30 years of experience in corporate research and development leadership and is recognized as a national leader in telecommunications.

Dr. Moradi is a winner of a 2012 R&D 100 Award for his wireless spectrum communication system innovation. He has been awarded four patents, and has one pending patent in wireless communications systems.